

# Arbitrary high-fidelity binomial codes from multiphoton spin-boson interactions

Pradip Laha<sup>1,\*</sup> and Peter van Loock<sup>1,†</sup>

<sup>1</sup>*Institute of Physics, Johannes Gutenberg-Universität Mainz, Staudingerweg 7, 55128 Mainz, Germany*

Encoding a qubit in the continuous degrees of freedom of a quantum system, such as bosonic modes, is a powerful alternative to modern quantum error correction (QEC). Among the most prominent bosonic QEC codes, binomial codes provide protection against loss and dephasing errors by encoding logical states in finite superpositions of Fock states with binomially weighted coefficients. While much attention has been given to their error-correcting capabilities and integration into fault-tolerant architectures, efficient methods for generating arbitrary binomial codewords remain scarce. In this work, we propose a scheme for generating these codewords by exploiting nonlinear multiphoton interactions between a continuous-variable bosonic mode (oscillator) and a two-level system (spin/qubit). Our proposed scheme assumes the ability to prepare the oscillator in an arbitrary Fock state and the qubit in an arbitrary superposition of its basis states and access to arbitrarily high multiphoton interactions. To enhance the experimental feasibility of our scheme, we further demonstrate how to reduce the required order parameter of multiphoton interactions by a factor of two for a special class of code states.

## I. INTRODUCTION

Quantum error correction (QEC) plays a foundational role in enabling scalable quantum information processing, providing a systematic framework to safeguard fragile quantum states from decoherence and other operational noise [1–5]. While conventional QEC schemes typically encode logical information into discrete-variable qubit registers, continuous-variable (CV) approaches leverage the infinite-dimensional Hilbert space structure of bosonic modes (or qumodes, such as quantized electromagnetic fields) to encode and protect quantum information [6–8]. Owing to their intrinsic redundancy and potential for resource-efficient error mitigation [9], CV-based error correction has attracted growing interest, making bosonic codes particularly promising for near-term quantum hardware where qubit resources are limited and noise is prevalent [10–22]. Prominent examples of encoding a qubit in bosonic modes include Gottesman-Kitaev-Preskill (GKP) codes [23–28], which protect against small displacement errors, and cat codes [29–34], which leverage coherent state superpositions to mitigate photon loss. These code states have demonstrated remarkable potential in experimental platforms such as superconducting circuits [12, 35–37], optical systems [38–40], and trapped ions [11, 18, 41].

Alongside these, binomial encoding [42] has emerged as a compelling alternative, offering protection against both photon loss and dephasing errors while requiring only modest hardware overhead [43]. These codes encode quantum information into *finite* superpositions of Fock states with binomially weighted amplitudes, carefully designed so that common error processes map codewords onto orthogonal, correctable states. Their discrete structure, analytical tractability, and compatibility with

bosonic modes make them highly attractive for near-term quantum technologies [12, 22, 44–50]. Binomial codes have been explored across a range of physical architectures, including superconducting circuits [12, 45, 47], light-matter systems [44], and trapped ions [11]. Recent studies have evaluated the fault tolerance and scalability of binomial codes under realistic noise [51]. Reference [48] examined concatenated architectures and identified photon-loss thresholds for different measurement strategies, while Ref. [52] proposes a scheme for logical qubit rotations within the binomial code space without the need for an ancillary qubit. Further, a quantum repeater architecture based on binomial codes has been proposed, employing a microwave cavity and a superconducting transmon to suppress photon loss while enabling high-fidelity state preparation and entanglement swapping [53]. In parallel, high-fidelity preparation of binomial code states has been experimentally demonstrated in a circuit-quantum electrodynamics (QED) architecture by employing transmon-mediated sideband interactions, enabling efficient multimode control and state encoding [54].

Despite significant progress, the high-fidelity generation of *arbitrary* binomial codewords remains a critical challenge. Most recent efforts to date have primarily focused on the simplest instance—protection against a single photon loss—where the two logical states of the qubit are given by  $|0\rangle = (|0\rangle + |4\rangle)/\sqrt{2}$  and  $|\bar{1}\rangle = |2\rangle$ , respectively. Here,  $|n\rangle$  is an  $n$ -photon Fock state ( $n = 0, 2, 4$ ). However, the general binomial code framework introduced in Ref. [43] enables protection against multiple photon loss, gain, and dephasing errors, albeit with increasingly complex logical encodings. Developing a universal, hardware-independent protocol for the high-fidelity preparation of arbitrary binomial codewords would mark a major step toward scalable, modular quantum architectures based on bosonic encodings.

In this work, we address this gap by introducing a protocol based on the multiphoton Jaynes–Cummings (MPJC) interaction, a highly nonlinear coupling between

\* plaha@uni-mainz.de

† loock@uni-mainz.de

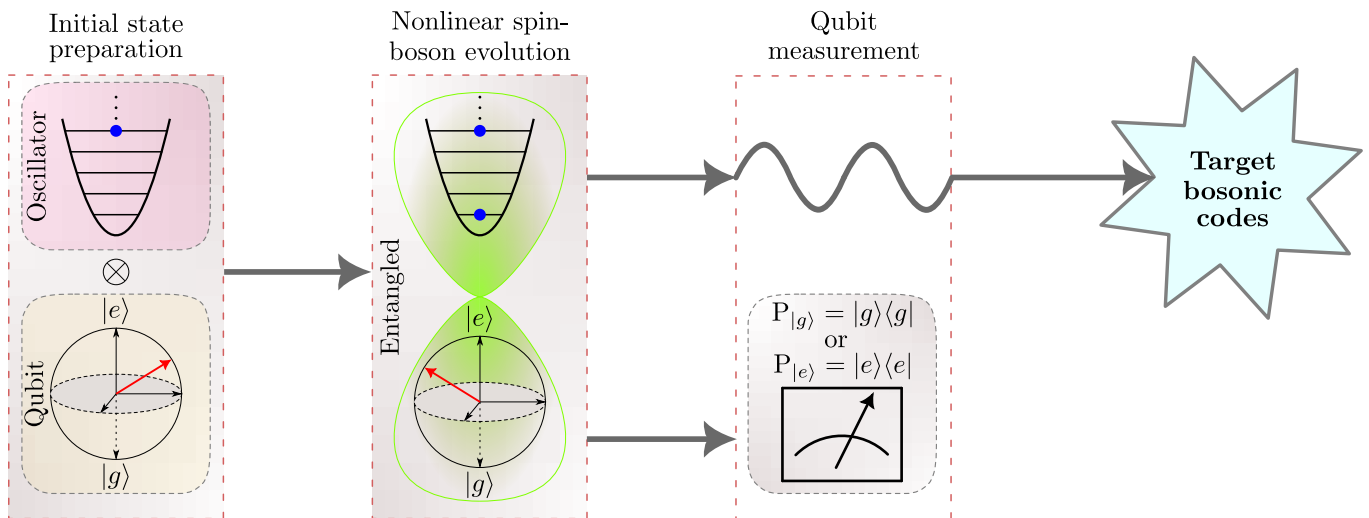


Figure 1. Schematic of the proposed protocol for synthesizing binomial code states composed of two Fock state superpositions. The protocol begins with state preparation, where the oscillator is initialized in a Fock state  $|n_1\rangle$  (blue solid circle) and the qubit in a superposition state  $\cos \theta |g\rangle + \sin \theta |e\rangle$  (red arrow). The joint system then undergoes an entangling evolution governed by a nonlinear multiphoton Jaynes–Cummings (MPJC) interaction of order  $m$ , mediated by a tunable coupling strength  $g$ . A projective measurement on the qubit at an optimized interaction time  $\tau$  collapses the oscillator into a nontrivial superposition of Fock states. The parameters  $n_1$ ,  $m$ ,  $\theta$ , and  $\tau$  uniquely determine the final encoded binomial state. The protocol can be recursively applied to construct more complex binomial states involving additional Fock components (see main text).

a two-level system (spin/qubit) and a bosonic mode. Initially developed in the context of nonlinear optics and cavity QED [55–59], MPJC-type Hamiltonians have seen renewed interest [60–64] due to their increasing experimental accessibility in quantum platforms such as superconducting circuits [65, 66] and trapped ions [67, 68].

Our approach exploits the nonlinearities inherent in the multiphoton generalization of the standard Jaynes–Cummings (JC) interaction to coherently drive the oscillator into arbitrary binomial codewords during its time evolution with high fidelity. Note that the standard JC interaction as directly available in cavity QED, including its dispersive regimes enabling spin-controlled phase rotations of an oscillator mode, has been shown [69] to be applicable for both cat code state engineering and cat code photon loss error syndrome identification. For the former, standard cavity QED interactions can be employed in an iterative fashion, starting from a *primitive state* [14]. It is tempting to consider a similar iterative approach to the generation of binomial code states. However, while the primitive state for the cat code is a simple coherent state, the primitive states associated with the binomial code are, from an experimental point of view, not really easier to realize than the target codewords themselves (see Appendix C for a brief discussion on this).

To achieve our objective, we assume initialization of the oscillator in a known Fock state and the qubit in an arbitrary superposition of its two basis states and access to tunable multiphoton interactions of arbitrary order. Under these conditions, and with appropriate local unitaries, we demonstrate high-fidelity synthesis of any bi-

nomial codeword (see Fig. 1). While our primary focus is on the probabilistic protocol—based on postselected qubit measurements—owing to its enhanced flexibility in parameter selection and higher achievable fidelities, we also demonstrate that similar target states can be synthesized deterministically by tracing out the qubit, albeit with a modest reduction in fidelity due to the mixedness introduced by this operation. Both analytical and numerical results confirm the scalability of our protocol to increasingly complex logical states.

It is instructive to contrast our protocol with schemes for GKP state generation in cavity and circuit QED, which typically rely on sequences of distinct interactions to engineer grid states in oscillator quadratures [70]. In contrast, our approach achieves deterministic preparation of structured bosonic codewords by tuning only the interaction time of a single MPJC Hamiltonian. While the resulting states form a comb in photon-number space rather than quadrature space, both protocols exploit controlled nonlinear light–matter interactions to generate highly nonclassical oscillator states.

While arbitrary oscillator Fock state preparation is now feasible across many quantum platforms [71–78], it is crucial to note that neither the standard nor multiphoton JC interactions can generate subsystem coherence from an initially incoherent joint state [59, 63, 79]. In our protocol, coherence in the spin state is therefore essential, as it seeds the coherence required in the initially incoherent oscillator state. Optimizing this initial spin coherence is consequently key to synthesizing the target bosonic state in a single step with high fidelity. A practical challenge in multiphoton protocols is the scaling of the required mul-

tiphoton order parameter with increasing code distance. To improve feasibility, we propose a two-step implementation that reduces the necessary photon-number requirement by a factor of two. This one-time improvement is achieved through judicious choices of initial conditions and by leveraging symmetries in the MPJC dynamics. Finally, to analyze the robustness of our scheme in realistic settings, we also briefly discuss the role of inevitable environmental-induced effects, including oscillator damping and qubit dephasing.

The remainder of this paper is organized as follows. Section II provides a short overview of the structure and properties of binomial codes. In Sec. III, we briefly introduce the MPJC Hamiltonian and describe the theoretical framework of our state-generation protocol. Sections IV and V present explicit constructions of binomial codewords involving two and three Fock components, respectively, using a probabilistic scheme. In Sec. VI, we examine how the required multiphoton parameter can be reduced, improving experimental feasibility. Section VII analyzes the impact of decoherence due to system–environment coupling on the fidelity of the generated states. The deterministic state generation protocol is discussed in Sec. VIII. We conclude in Sec. IX with a brief summary and outlook. Supplementary technical details and extended results are provided in the appendixes.

## II. BINOMIAL CODE STATES

As noted earlier, the generic binomial code encodes the two logical qubit states into *finite* superpositions of Fock states with binomially distributed amplitudes. It was first introduced in Ref. [43] as a two-parameter  $(N, K)$  code space to correct against up to  $L$  photon losses, up to  $G$  photon gain errors, and  $D$  dephasing events. Here,  $N = L + G + 1$  decides the spacing of the superpositions of Fock states, and  $K = \max\{L, G, 2D\} + 1$  is responsible for the number of Fock states that are present in the superposition. The generic class of the two logical states is defined as

$$|\bar{0}\rangle_{N,K} = \frac{1}{\sqrt{2^{K-1}}} \sum_{k=0}^{\lfloor \frac{K}{2} \rfloor} \sqrt{\binom{K}{2k}} |2kN\rangle, \quad (1a)$$

$$|\bar{1}\rangle_{N,K} = \frac{1}{\sqrt{2^{K-1}}} \sum_{k=0}^{\lfloor \frac{K-1}{2} \rfloor} \sqrt{\binom{K}{2k+1}} |(2k+1)N\rangle, \quad (1b)$$

where,  $\lfloor \cdot \rfloor$  denotes the conventional floor function [48]. For simplicity, we neglect photon gain errors in this work (i.e.,  $G = 0$ ), such that  $N = L + 1$  and  $K = \max\{L, 2D\} + 1$ . For a fixed value of  $L$ , the number of correctable dephasing errors is determined by  $K$ . In the asymptotic limit  $K \rightarrow \infty$ , the binomial codes asymptotically approach the  $2(L+1)$ -legged cat codes [30–33], which are known to protect against up to  $L$  photon loss

errors, as discussed in Ref. [43]. Both binomial and cat codes belong to the broader class of rotation-symmetric bosonic codes (RSBCs) [14, 51, 80], characterized by their invariance under discrete rotations by a fixed angle in phase space. In this context, the parameter  $N$  quantifies the degree of discrete rotation symmetry for the code.

The simplest and most well-known instance—mentioned in the previous section—corresponds to the case  $L = 1$ , which corrects a single photon loss. The associated logical states are  $|\bar{0}\rangle_{2,2} = \frac{1}{\sqrt{2}}(|0\rangle + |4\rangle)$ , and  $|\bar{1}\rangle_{2,2} = |2\rangle$ , where  $K = 2$ . By fixing  $L = 1$  and increasing  $K$ , one obtains codewords that maintain protection against single photon loss while improving resilience to dephasing. On the other hand, the lowest-order binomial codewords capable of correcting up to two photon loss events ( $L = 2$ ) are  $|\bar{0}\rangle_{3,3} = \frac{1}{2}(|0\rangle + \sqrt{3}|6\rangle)$  and  $|\bar{1}\rangle_{3,3} = \frac{1}{2}(\sqrt{3}|3\rangle + |9\rangle)$ . Higher-order encoded states corresponding to larger  $N$  and  $K$  values can be systematically constructed from Eq. (1). The objective of this work is to produce arbitrary superpositions of these Fock states with high fidelity.

## III. MULTIPHOTON SPIN-BOSON HAMILTONIAN

The JC model [81, 82] captures the fundamental physics of light–matter interactions and forms the basis for understanding cavity and circuit QED systems. It plays a central role in the theoretical and experimental development of quantum optics and quantum information platforms [83]. The standard JC model describes the coherent coupling between a two-level system (spin) and a single quantized harmonic oscillator mode (boson). The two states of the qubit,  $|g\rangle$  and  $|e\rangle$ , are assumed to be separated by a transition frequency  $\omega_0$ , while the oscillator is characterized by respective bosonic creation and annihilation operators  $a^\dagger$  and  $a$ , with mode frequency  $\omega$ . The detuning is typically denoted as  $\Delta = \omega_0 - \omega$ . The free energy Hamiltonian is expressed as  $H_0 = \frac{\omega_0}{2}\sigma_z + \omega a^\dagger a$  while the interaction Hamiltonian is given by  $H_{\text{int}} = g(a\sigma_+ + a^\dagger\sigma_-)$  where  $g$  denotes the strength of the spin-boson interaction. Here,  $\sigma_z = |e\rangle\langle e| - |g\rangle\langle g|$ ,  $\sigma_+ = |e\rangle\langle g|$ ,  $\sigma_- = |g\rangle\langle e|$  are the standard spin operators. The total Hamiltonian is therefore  $H = H_0 + H_{\text{int}}$ . It is often useful to split  $H$  into two mutually commuting terms as  $H = H_I + H_{II}$ , where  $H_I = \omega(a^\dagger a + \frac{\sigma_z}{2})$  and  $H_{II} = \frac{\Delta}{2}\sigma_z + H_{\text{int}}$ . In the limit  $\Delta = 0$  (on resonance),  $H_{II} \equiv H_{\text{int}}$ .

Over the years, the standard JC model has been extended in various directions to capture richer quantum phenomena (see Ref. [83] for a review). Among these, the multiphoton generalization is particularly notable [55–58, 60]. The MPJC model describes a coherent exchange of  $m$  bosonic excitations with a two-level system. Its interaction Hamiltonian is given by

$$H_{\text{int}} = ig(a^m\sigma_+ - a^{\dagger m}\sigma_-), \quad (2)$$

where  $m$  is the multiphoton order parameter and  $g$  is the effective coupling strength. Note that the interaction Hamiltonian  $H_{\text{int}}$  in Eq. (2) is equivalent to the conventional form  $H'_{\text{int}} = g(a^m \sigma_+ + a^{\dagger m} \sigma_-)$ , differing only by a phase convention for the two-level system operators and, correspondingly, for the coupling constant. Specifically, applying the transformation  $\sigma_- \rightarrow e^{i\phi} \sigma_-$  (and  $\sigma_+ \rightarrow e^{-i\phi} \sigma_+$ ) in  $H'_{\text{int}}$  and choosing  $\phi = \pi/2$  recovers  $H_{\text{int}}$ . The case  $m = 1$  corresponds to the standard JC model. In what follows, we will find out that  $m$  plays a crucial role in engineering the desired quantum superposition states. Throughout this work, we restrict ourselves to the resonant regime  $\Delta = \omega_0 - m\omega = 0$ , where the MPJC dynamics admits a transparent analytical solution and directly enables the state-engineering protocols discussed below. Extensions of the protocol to finite detuning  $\Delta \neq 0$  are in principle possible but require a separate analysis and are beyond the scope of the present work.

We mention in passing a recent circuit QED demonstration of single-mode control over cavity modes by preparing both Fock states  $|n\rangle$  and vacuum-Fock superpositions  $(|0\rangle + |n\rangle)/\sqrt{2}$  by climbing the JC ladder with transmon rotations and sideband pulses. Fock states are prepared using a sequence of broadband pulses followed by sideband  $\pi$  pulses. Consequently, a shelving method is employed to achieve superposition states [54].

### A. Time-evolved state of the MPJC Hamiltonian

Before proceeding, we summarize the key assumptions of our state preparation protocol, as introduced earlier: (i) the oscillator is initialized in a Fock state  $|n_1\rangle$ , while the qubit starts in an arbitrary superposition  $|\psi_q(\theta)\rangle = \cos\theta|g\rangle + \sin\theta|e\rangle$ ; (ii) tunable access to MPJC interactions ( $H_{\text{int}}$  in Eq. (2)) with arbitrary  $m$  is available; and (iii) projective qubit measurements can be performed at chosen times during the evolution dictated by the target state. Under these assumptions, the binomial target state preparation protocol can be succinctly summarized as

$$|\psi_o\rangle_{\text{target}} \propto \langle g/e| e^{-iH_{\text{int}}\tau} (|\psi_q(\theta)\rangle \otimes |\psi_o(0)\rangle). \quad (3)$$

Notably, we will later show that employing a two-step generation protocol—rather than a single-step approach—can reduce the required value of  $m$  by a factor of two, significantly easing experimental demands.

According to the first assumption, the initial joint state of the system can be written as

$$|\Psi(0)\rangle = \cos\theta|g, n_1\rangle + \sin\theta|e, n_1\rangle, \quad (4)$$

where the notation is self-evident. It is important to emphasize that neither the standard JC Hamiltonian nor its multiphoton generalization (MPJC) can generate coherence within either subsystem if the joint system initially

lacks coherence [63, 79]. In the case of the spin, this is because  $H_{\text{int}}$  merely rotates the Bloch vector trivially along the  $z$ -axis [79]. As we will demonstrate, initial coherence in the qubit (parametrized by the angle  $\theta$ ) is essential for generating the desired superpositions in the oscillator.

We now turn to the time-evolved state vector  $|\psi(t)\rangle$ , governed by the interaction Hamiltonian  $H_{\text{int}}$  in Eq. (2), starting from a pure initial product state  $|\psi(0)\rangle$  in Eq. (4). It is straightforward to show that the evolved state has the form

$$|\Psi(\tau)\rangle = x_1(\tau)|g, n_1\rangle + x_2(\tau)|e, n_1\rangle + x_3(\tau)|g, n_1 + m\rangle + x_4(\tau)|e, n_1 - m\rangle, \quad (5)$$

where the time-dependent coefficients are found to be

$$x_1(\tau) = \cos\theta \cos\left(\sqrt{n_1!/(n_1 - m)!}\tau\right), \quad (6a)$$

$$x_2(\tau) = \sin\theta \cos\left(\sqrt{(n_1 + m)!/n_1!}\tau\right), \quad (6b)$$

$$x_3(\tau) = -\sin\theta \sin\left(\sqrt{(n_1 + m)!/n_1!}\tau\right), \quad (6c)$$

$$x_4(\tau) = \cos\theta \sin\left(\sqrt{n_1!/(n_1 - m)!}\tau\right), \quad (6d)$$

for  $n_1 \geq m$ . When  $n_1 < m$ ,  $x_1(\tau) = \cos\theta$ ,  $x_4(\tau) = 0$ . Here,  $\tau = gt$  denotes the dimensionless scaled interaction time (see Appendix A for details).

### IV. SUPERPOSITION OF TWO FOCK STATES

It can be readily verified from Eq. (1) that there are eight logical states in total, each being a superposition of only two Fock states, given by

$$|\bar{0}\rangle_{2,2} = \frac{1}{\sqrt{2}}(|0\rangle + |4\rangle), \quad (7a)$$

$$|\bar{0}\rangle_{2,3} = \frac{1}{2}(|0\rangle + \sqrt{3}|4\rangle), \quad (7b)$$

$$|\bar{1}\rangle_{2,3} = \frac{1}{2}(\sqrt{3}|2\rangle + |6\rangle), \quad (7c)$$

$$|\bar{1}\rangle_{2,4} = \frac{1}{\sqrt{2}}(|2\rangle + |6\rangle), \quad (7d)$$

$$|\bar{0}\rangle_{3,3} = \frac{1}{2}(|0\rangle + \sqrt{3}|6\rangle), \quad (7e)$$

$$|\bar{1}\rangle_{3,3} = \frac{1}{2}(\sqrt{3}|3\rangle + |9\rangle), \quad (7f)$$

$$|\bar{1}\rangle_{3,4} = \frac{1}{\sqrt{2}}(|3\rangle + |9\rangle), \quad (7g)$$

$$|\bar{1}\rangle_{4,4} = \frac{1}{\sqrt{2}}(|4\rangle + |12\rangle). \quad (7h)$$

In the following, we exploit the joint state  $|\Psi(\tau)\rangle$  in Eq. (5) to generate all eight superpositions states. Our main protocol is probabilistic, relying on projective measurement of the qubit to herald the target oscillator state. We focus on this approach due to its ability to achieve higher fidelities and greater flexibility in parameter selection. For completeness, we also examine a deterministic generation protocol that avoids qubit measurement by tracing over the qubit degrees of freedom. The details

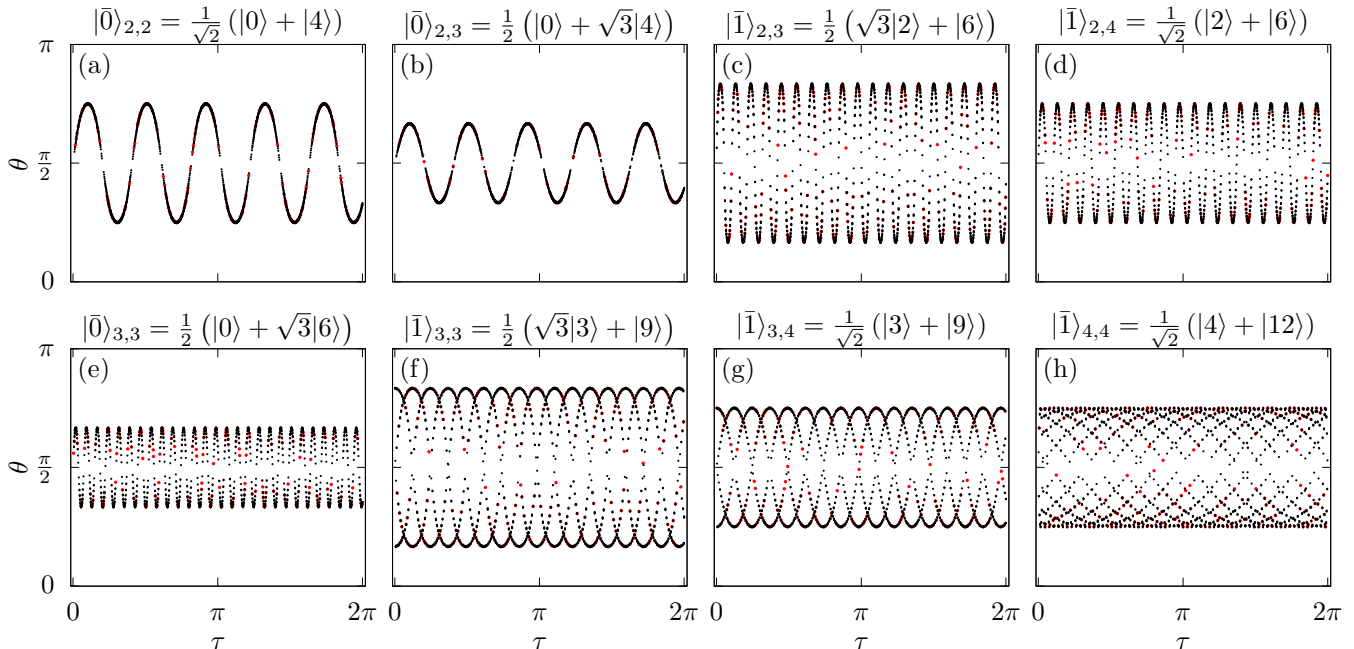


Figure 2. Combinations of  $\{\tau, \theta\}$  for which the fidelity  $F_{2g}(\tau, \theta)$  of the postselected oscillator state—obtained by measuring the qubit in the ground state  $|g\rangle$  and given in Eq. (9)—matches each of the eight target logical binomial states with unit fidelity are shown in panels (a)–(h), respectively. The parameters  $\tau$  and  $\theta$  were sampled uniformly over  $0 \leq \tau \leq 2\pi$  and  $0 \leq \theta \leq \pi$ , using 1001 and 501 points, respectively. All displayed points satisfy a numerical fidelity threshold of  $|F_{2g} - 1| \leq 10^{-4}$ , with red points marking those that additionally meet the stricter threshold  $|F_{2g} - 1| \leq 10^{-6}$ .

of this alternative method, along with its limitations and comparative performance, are discussed in Sec. VIII.

Upon projective measurement of the qubit, if it is found in the ground state  $|g\rangle$ , the corresponding unnormalized oscillator state is given by  $|\psi_o(\tau)\rangle_{2g} = x_1(\tau)|n_1\rangle + x_3(\tau)|n_1 + m\rangle$ , as follows directly from Eq. (5). It is important to note that obtaining the eight superposition states in Eq. (7) from  $|\psi_o(\tau)\rangle_{2g}$  requires  $m > n_1$ . Therefore, we have

$$|\psi_o(\tau)\rangle_{2g} = \mathcal{N}_{2g} \{ \cos \theta |n_1\rangle - \sin \theta \sin(a_{n_1, m} \tau) |n_1 + m\rangle \}, \quad (8)$$

where  $a_{n_1, m} = \sqrt{(n_1 + m)!/n_1!}$  and the normalization  $\mathcal{N}_{2g} = \{ \cos^2 \theta + \sin^2 \theta \sin^2(a_{n_1, m} \tau) \}^{-1/2}$ .

Writing the eight target states in the form  $c_0 |n_1\rangle + c_1 |n_1 + m\rangle$  (where  $|c_0|^2 + |c_1|^2 = 1$ ), we can express the fidelity in the generic compact form

$$F_{2g}(\tau, \theta) = \frac{|c_0 \cos \theta - c_1 \sin \theta \sin(a_{n_1, m} \tau)|^2}{\cos^2 \theta + \sin^2 \theta \sin^2(a_{n_1, m} \tau)}. \quad (9)$$

By judiciously choosing the pair  $(n_1, m)$  one selects which member of the two-Fock-component binomial code family is to be realized. Once the values of  $n_1$ , and  $m$  are fixed, the remaining task is to optimize the control parameters  $\theta$  and  $\tau$ , which determine the relative weights of the two Fock components, to achieve fidelities arbitrary close to unity. Although the states  $|\psi_o(\tau)\rangle_{2g}$  in Eq. (8) span the relevant two-dimensional Fock subspace, identi-

Table I. Counts of parameter pairs  $(\tau, \theta)$  for which the fidelity  $F_{2g}$  (see Eq. (9)) between the engineered two-Fock-component state in Eq. (8) and the corresponding eight target codeword satisfies  $|F_{2g} - 1| \leq 10^{-4}$  or  $10^{-6}$ . The parameters  $\tau$  and  $\theta$  were sampled uniformly over  $0 \leq \tau \leq 2\pi$  and  $0 \leq \theta \leq \pi$ , using 1001 and 501 points, respectively. Each entry reports the number of grid points in the scanned  $(\tau, \theta)$  domain for which the fidelity falls within the specified tolerance.

State	$N_{10^{-4}}$	$N_{10^{-6}}$	State	$N_{10^{-4}}$	$N_{10^{-6}}$
$ 0\rangle_{2,2}$	2545	271	$ 0\rangle_{3,3}$	2217	217
$ \bar{0}\rangle_{2,3}$	2233	219	$ \bar{1}\rangle_{3,3}$	3081	291
$ \bar{1}\rangle_{2,3}$	3094	298	$ \bar{1}\rangle_{3,4}$	2520	270
$ \bar{1}\rangle_{2,4}$	2522	271	$ \bar{1}\rangle_{4,4}$	2504	260

fying the corresponding control parameters generally requires a numerical search. This is due to the fact that the effective coupling strength  $a_{n_1, m}$  is typically irrational, preventing a closed-form analytical solution for arbitrary target amplitude ratios. We therefore perform a numerical optimization numerically by scanning  $\theta \in [0, \pi]$ , and  $\tau \in [0, 2\pi]$  with a resolution of 501 points for  $\theta$  and 1001 points for  $\tau$ . Numerous parameter combinations yield fidelities equal to unity for all eight states, highlighting the robustness and flexibility of the protocol.

These optimal combinations are visualized in Fig. 2, where each scatter point corresponds to a distinct choice of  $(\theta, \tau)$  achieving unit fidelity under the numerical tol-

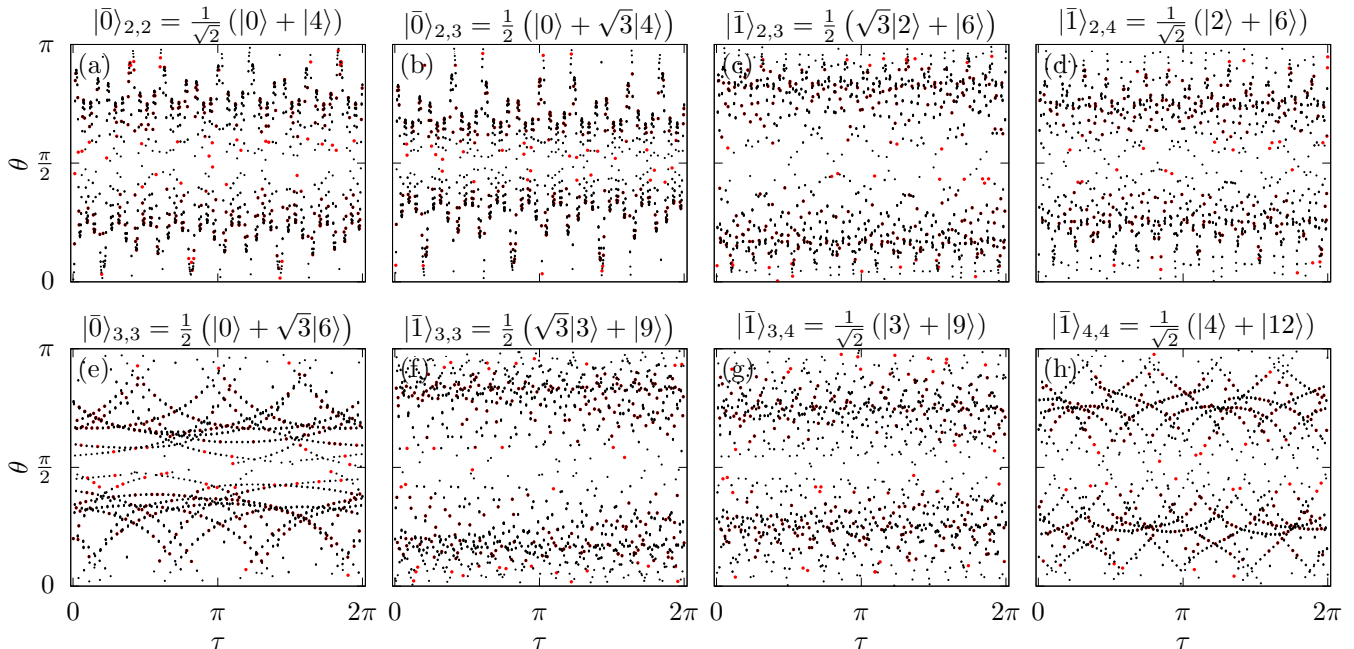


Figure 3. Combinations of  $\{\tau, \theta\}$  for which the fidelity  $F_{2e}(\tau, \theta)$  of the postselected oscillator state—obtained by measuring the qubit in the ground state  $|e\rangle$  and given in Eq. (11)—matches each of the eight target logical binomial states with unit fidelity are shown in panels (a)–(h), respectively. All sampling details and fidelity thresholds are identical to those used in Fig. 2.

erance of  $10^{-4}$ . As anticipated, tightening the precision requirement reduces the number of admissible solutions: under a stricter tolerance of  $10^{-6}$ , only the most robust matches survive, shown as red points in the plots. The details on the total count of the optimal parameter pairs are listed in Table I for all eight cases.

On the other hand, if the qubit is in the excited state  $|e\rangle$  after measurement, the resulting oscillator state has the form

$$|\psi_o(\tau)\rangle_{2e} = \mathcal{N}_{2e} \left\{ \sin \theta \cos(a_{n_1, m} \tau) |n_1\rangle + \cos \theta \sin(b_{n_1, m} \tau) |n_1 - m\rangle \right\}, \quad (10)$$

where  $b_{n_1, m} = \sqrt{n_1!/(n_1 - m)!}$  and the normalization  $\mathcal{N}_{2e} = \left\{ \cos^2 \theta \sin^2(a_{n_1, m} \tau) + \sin^2 \theta \cos^2(b_{n_1, m} \tau) \right\}^{-\frac{1}{2}}$ .

Once again, with judicious choices of  $n_1$  and  $m$  ( $n_1 \geq m$ ), and by appropriately tuning the control parameters  $\theta$  and  $\tau$ , all eight target two-Fock superposition states can be systematically synthesized. As before, although these parameters provide full control over the two-dimensional Fock subspace, identifying those that realize a given target state generally requires a numerical optimization due to the irrational effective coupling strengths  $a_{n_1, m}$  and  $b_{n_1, m}$ . Writing the target states in the form  $c_0 |n_1 - m\rangle + c_1 |n_1\rangle$ , the fidelity assumes the compact expression

$$F_{2e}(\tau, \theta) = \frac{|c_0 \cos \theta \sin(b_{n_1, m} \tau) + c_1 \sin \theta \cos(a_{n_1, m} \tau)|^2}{\cos^2 \theta \sin^2(b_{n_1, m} \tau) + \sin^2 \theta \cos^2(a_{n_1, m} \tau)}. \quad (11)$$

Similar to the previous case, we find multiple parameter combinations that achieve all the target binomial code states with unit fidelity, as illustrated in Fig. 3. The corresponding counts of optimal parameter choices are detailed in Table II.

It is straightforward to verify that, by following a similar procedure, arbitrary superpositions of two Fock states can be realized (see Appendix B for further details). In the following section, we extend this approach to generate superpositions of three Fock states.

Table II. Counts of parameter pairs  $(\tau, \theta)$  for which the fidelity  $F_{2e}$  (see Eq. (11)) satisfies  $|F_{2e} - 1| \leq 10^{-4}$  or  $10^{-6}$ . The remaining details are the same as in Table I.

State	$N_{10^{-4}}$	$N_{10^{-6}}$	State	$N_{10^{-4}}$	$N_{10^{-6}}$
$ 0\rangle_{2,2}$	2347	267	$ 0\rangle_{3,3}$	2508	265
$ \bar{0}\rangle_{2,3}$	2514	255	$ \bar{1}\rangle_{3,3}$	2381	228
$ \bar{1}\rangle_{2,3}$	2502	255	$ \bar{1}\rangle_{3,4}$	2521	248
$ \bar{1}\rangle_{2,4}$	2375	242	$ \bar{1}\rangle_{4,4}$	2366	253

## V. SUPERPOSITION OF THREE FOCK STATES

A straightforward inspection of Eq. (1) reveals that there exist sixteen logical states in total, each being a superposition of only three Fock states. Out of which the seven logical  $|\bar{0}\rangle$  states (3 for  $K = 4$  and 4 for  $K = 5$ )

are given by

$$|\bar{0}\rangle_{N,4} = \frac{1}{2\sqrt{2}} \left( |0\rangle + \sqrt{6}|2N\rangle + |4N\rangle \right), \quad (12a)$$

$$|\bar{0}\rangle_{N,5} = \frac{1}{4} \left( |0\rangle + \sqrt{10}|2N\rangle + \sqrt{5}|4N\rangle \right). \quad (12b)$$

The remaining nine logical  $|\bar{1}\rangle$  states (4 for  $K = 5$  and 5 for  $K = 6$ ) are given by

$$|\bar{1}\rangle_{N,5} = \frac{1}{4} \left( \sqrt{5}|N\rangle + \sqrt{10}|3N\rangle + |5N\rangle \right), \quad (13a)$$

$$|\bar{1}\rangle_{N,6} = \frac{1}{4\sqrt{2}} \left( \sqrt{6}|N\rangle + \sqrt{20}|3N\rangle + \sqrt{6}|5N\rangle \right). \quad (13b)$$

In all cases,  $N = 2, 3, \dots, K$ .

In the preceding section, we demonstrated that, by employing the MPJC Hamiltonian and appropriately selecting the initial configurations, arbitrary superpositions of two Fock states can be engineered. In what follows, we extend this method to synthesize superpositions of three Fock states with high fidelity, by using an initial oscillator state that is itself an arbitrary superposition of two Fock states, along with an initial arbitrary superposition of the qubit basis states. That is, we assume the initial state for the bipartite system to be

$$|\Psi(0)\rangle = (\cos\theta|g\rangle + \sin\theta|e\rangle) \otimes (\cos\phi|n_1\rangle + \sin\phi|n_2\rangle). \quad (14)$$

It is worth noting that, although such an initial state formally departs from our first assumption, we showed in the previous section that arbitrary two-Fock superpositions can still be generated using the MPJC Hamiltonian. Building on this, three-Fock-state superpositions can be realized in a two-step protocol: first prepare a two-Fock resource state, then extend it to the desired three-Fock superposition. It can be straightforwardly shown that the corresponding time-evolved state can be written compactly as a superposition of two independent two-Fock dynamical blocks. Explicitly, one finds

$$|\Psi(\tau)\rangle = \sum_{i=1}^4 x_i(\tau) |\chi_i(n_1)\rangle + \sum_{i=1}^4 y_i(\tau) |\chi_i(n_2)\rangle, \quad (15)$$

where  $|\chi_i(n)\rangle \in |g, n\rangle, |e, n\rangle, |g, n+m\rangle, |e, n-m\rangle$ . The time-dependent amplitudes factorize as

$$x_i(\tau) = \cos\phi x_i^{(2)}(n_1, m, \theta, \tau), \quad (16a)$$

$$y_i(\tau) = \sin\phi x_i^{(2)}(n_2, m, \theta, \tau), \quad (16b)$$

where  $x_i^{(2)}$  denotes the coefficients of the two-Fock solution given previously in Eq. (6). Thus the three-Fock evolution decomposes naturally into two independent excitation manifolds, weighted by  $\cos\phi$  and  $\sin\phi$ , respectively. For  $n_1 < m$ ,  $x_1(\tau) = \cos\theta \cos\phi$ ,  $x_4(\tau) = 0$  and for  $n_2 < m$ ,  $y_1(\tau) = \cos\theta \sin\phi$ ,  $y_4(\tau) = 0$  (see Appendix A for details). The two-Fock solution is recovered simply by setting  $\phi = 0$ .

Table III. The coefficients  $C_{lg}^{(\pm)}$  and  $C_{le}^{(\pm)}$  for the three-Fock-component states. Note that  $a_{n_1, m} = \sqrt{(n_1 + m)!/n_1!}$ ,  $b_{n_1, m} = \sqrt{n_1!/(n_1 - m)!}$ , and  $c_{n_1, m} = \sqrt{(n_1 + 2m)!/(n_1 + m)!}$ .

$C_{0g}^{(+)}$	$\cos\theta \cos\phi$
$C_{1g}^{(+)}$	$\cos\theta \sin\phi \cos(a_{n_1, m}\tau) - \sin\theta \cos\phi \sin(a_{n_1, m}\tau)$
$C_{2g}^{(+)}$	$-\sin\theta \sin\phi \sin(c_{n_1, m}\tau)$
$C_{0g}^{(-)}$	$\cos\theta \sin\phi$
$C_{1g}^{(-)}$	$\cos\theta \cos\phi \cos(b_{n_1, m}\tau) - \sin\theta \sin\phi \sin(b_{n_1, m}\tau)$
$C_{2g}^{(-)}$	$-\sin\theta \cos\phi \sin(a_{n_1, m}\tau)$
$C_{0e}^{(+)}$	$\cos\theta \cos\phi \sin(b_{n_1, m}\tau)$
$C_{1e}^{(+)}$	$\sin\theta \cos\phi \cos(a_{n_1, m}\tau) + \cos\theta \sin\phi \sin(a_{n_1, m}\tau)$
$C_{2e}^{(+)}$	$\sin\theta \sin\phi \cos(c_{n_1, m}\tau)$
$C_{0e}^{(-)}$	$\cos\theta \sin\phi$
$C_{1e}^{(-)}$	$\cos\theta \cos\phi \sin(b_{n_1, m}\tau) + \sin\theta \sin\phi \cos(b_{n_1, m}\tau)$
$C_{2e}^{(-)}$	$\sin\theta \cos\phi \cos(a_{n_1, m}\tau)$

Now, suppose a projective measurement is performed on the qubit, and the outcome is the ground state  $|g\rangle$ . The oscillator is then projected onto a four-Fock superposition state given by

$$|\psi_o(\tau)\rangle_{4g} = \mathcal{N}_{4g} \left\{ x_1(\tau) |n_1\rangle + x_3(\tau) |n_1 + m\rangle + y_1(\tau) |n_2\rangle + y_3(\tau) |n_2 + m\rangle \right\}, \quad (17)$$

where  $\mathcal{N}_{4g}$  is the normalization factor.

The four-Fock component superposition state in Eq. (17) can be reduced to a three distinct components only when the pairs  $\{n_1, n_1 + m\}$  and  $\{n_2, n_2 + m\}$  overlap on exactly one element. Given that all Fock numbers are nonnegative integers, two possibilities arise. These are (i)  $n_2 = n_1 + m$ , and (ii)  $n_2 = n_1 - m$  (with  $n_1 \geq m$ ).

In the case  $n_2 = n_1 + m$ , the accessible Fock ladder is  $k_0, k_1, k_2 = n_1, n_1 + m, n_1 + 2m$ . Note that for all the sixteen logical states, this requires  $n_1 < m$  (see Eqs. (12) and (13)). For the alternative choice  $n_2 = n_1 - m$  with  $n_1 \geq m$ , the ladder becomes  $k_0, k_1, k_2 = n_1 - m, n_1, n_1 + m$ . In both cases, the oscillator state derived from Eq. (17) can be written in the unified form

$$|\psi_o(\tau)\rangle_{3g\pm} = \mathcal{N}_{3g\pm} \sum_{l=0}^2 C_{lg}^{(\pm)}(\tau, \theta, \phi) |k_l\rangle, \quad (18)$$

where the choice of  $k_0, k_1, k_2$  is determined by whether  $n_2 = n_1 + m$  ('+') or  $n_2 = n_1 - m$  ('-'). The exact expressions of the coefficients  $C_{lg}^{(\pm)}$  can be found in Table III. The normalization factor  $\mathcal{N}_{3g\pm} = \left\{ |C_{0g}^{(\pm)}|^2 + |C_{1g}^{(\pm)}|^2 + |C_{2g}^{(\pm)}|^2 \right\}^{-1/2}$ .

Writing the sixteen target states in the form  $\sum_l c_l |k_l\rangle$  for both the cases, the fidelity for both constructions can

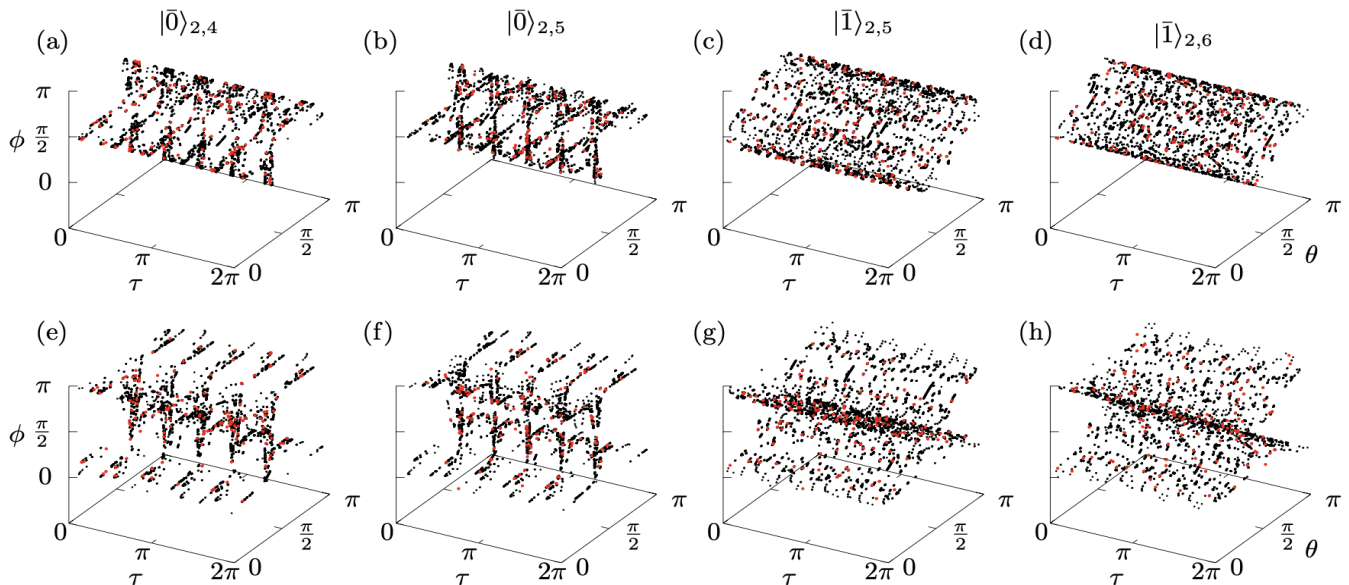


Figure 4. Combinations of  $\{\tau, \theta, \phi\}$  for which the fidelity ( $F_{3g_{\pm}}$  in Eq. (19)) of the postselected oscillator state in Eq. (18) reaches unity (within numerical precision) with each of the four three-component binomial targets  $|\bar{0}\rangle_{2,4} = \frac{1}{2\sqrt{2}}(|0\rangle + \sqrt{6}|4\rangle + |8\rangle)$ ,  $|\bar{0}\rangle_{2,5} = \frac{1}{4}(|0\rangle + \sqrt{10}|4\rangle + \sqrt{5}|8\rangle)$ ,  $|\bar{1}\rangle_{2,5} = \frac{1}{4}(\sqrt{5}|2\rangle + \sqrt{10}|6\rangle + |10\rangle)$ , and  $|\bar{1}\rangle_{2,6} = \frac{1}{4\sqrt{2}}(\sqrt{6}|2\rangle + \sqrt{20}|6\rangle + \sqrt{6}|10\rangle)$  are shown. The top row corresponds to the case  $n_2 = n_1 + m$  ( $F_{3g_+}$ ), while the bottom row corresponds to  $n_2 = n_1 - m$  ( $F_{3g_-}$ ). The parameters were sampled uniformly over  $0 \leq \tau \leq 2\pi$  (1001 points) and  $0 \leq \theta, \phi \leq \pi$  (501 points each). As in Figs. 2 and 3, all plotted points satisfy  $|F - 1| \leq 10^{-4}$ , with red points indicating those additionally meeting the stricter threshold  $|F - 1| \leq 10^{-6}$ .

be succinctly expressed in the form

$$F_{3g_{\pm}}(\tau, \theta, \phi) = \frac{\left| \sum_{l=0}^2 c_l C_{lg}^{(\pm)}(\tau, \theta, \phi) \right|^2}{\sum_{l=0}^2 \left| C_{lg}^{(\pm)}(\tau, \theta, \phi) \right|^2}. \quad (19)$$

In what follows, we illustrate the procedure using four representative examples: the binomial code states  $|\bar{0}\rangle_{2,4}$ ,  $|\bar{0}\rangle_{2,5}$ ,  $|\bar{1}\rangle_{2,5}$ , and  $|\bar{1}\rangle_{2,6}$ . The first pair are superpositions of  $|0\rangle$ ,  $|4\rangle$ , and  $|8\rangle$ , while the second pair are superpositions of  $|2\rangle$ ,  $|6\rangle$ , and  $|10\rangle$ . For the choice  $n_2 = n_1 + m$ , these pairs correspond to  $n_1 = 0$  and  $n_1 = 2$ , respectively. For the alternative choice  $n_2 = n_1 - m$ , they correspond instead to  $n_1 = 4$  and  $n_1 = 6$ . In both constructions, the spacing is fixed at  $m = 4$ .

Similar to the two-Fock-component case, the task now reduces to optimizing the control parameters—here  $\theta$ ,  $\phi$ , and  $\tau$ —to achieve unit fidelity for each target code state. This optimization is again performed numerically. As explained before, this numerical search is necessitated by the generally irrational nature of the effective coupling strengths, which prevents a closed-form analytical determination of the control parameters for arbitrary target states. Specifically, we scan the parameter ranges  $\theta \in [0, \pi]$ ,  $\phi \in [0, \pi]$ , and  $\tau \in [0, 2\pi]$  using a grid of 501 points for  $\theta$  and  $\phi$ , and 1001 points for  $\tau$ . As in the two-Fock case, a large number of parameter triples yield unit fidelities, up to numerical precision. These

Table IV. Counts of parameter triplets  $(\tau, \theta, \phi)$  for which the fidelity  $F_{3g_{\pm}}$  (see Eq. (19)) between the engineered three-Fock-component state in Eq. (18) and the corresponding sixteen target codeword satisfies  $|F_{3g_{\pm}} - 1| \leq 10^{-4}$  or  $10^{-6}$ . The parameters  $\tau$ ,  $\theta$ , and  $\phi$  were sampled uniformly over  $0 \leq \tau \leq 2\pi$ ,  $0 \leq \theta \leq \pi$  and  $0 \leq \phi \leq \pi$ , using 1001, 501 and 501 points, respectively. Each entry reports the number of grid points in the scanned  $(\tau, \theta, \phi)$  domain for which the fidelity falls within the specified tolerance.

$n_2 = n_1 + m$			$n_2 = n_1 - m$		
State	$N_{10^{-4}}$	$N_{10^{-6}}$	State	$N_{10^{-4}}$	$N_{10^{-6}}$
$ \bar{0}\rangle_{2,4}$	13097	147	$ \bar{0}\rangle_{2,4}$	13097	147
$ \bar{0}\rangle_{2,5}$	12418	135	$ \bar{0}\rangle_{2,5}$	12418	135
$ \bar{1}\rangle_{2,5}$	16297	161	$ \bar{1}\rangle_{2,5}$	16297	161
$ \bar{1}\rangle_{2,6}$	13908	144	$ \bar{1}\rangle_{2,6}$	13908	144

optimal combinations are visualized as scatter plots in Fig. 4, highlighting the substantial flexibility in selecting parameters for synthesizing the target code states. As expected, increasing the numerical precision to  $10^{-6}$  reduces the number of viable solutions (marked as red points in the plots). Further details are provided in Table IV.

On the other hand, after the measurement, if the qubit is found in the excited state  $|e\rangle$ , the oscillator gets pro-

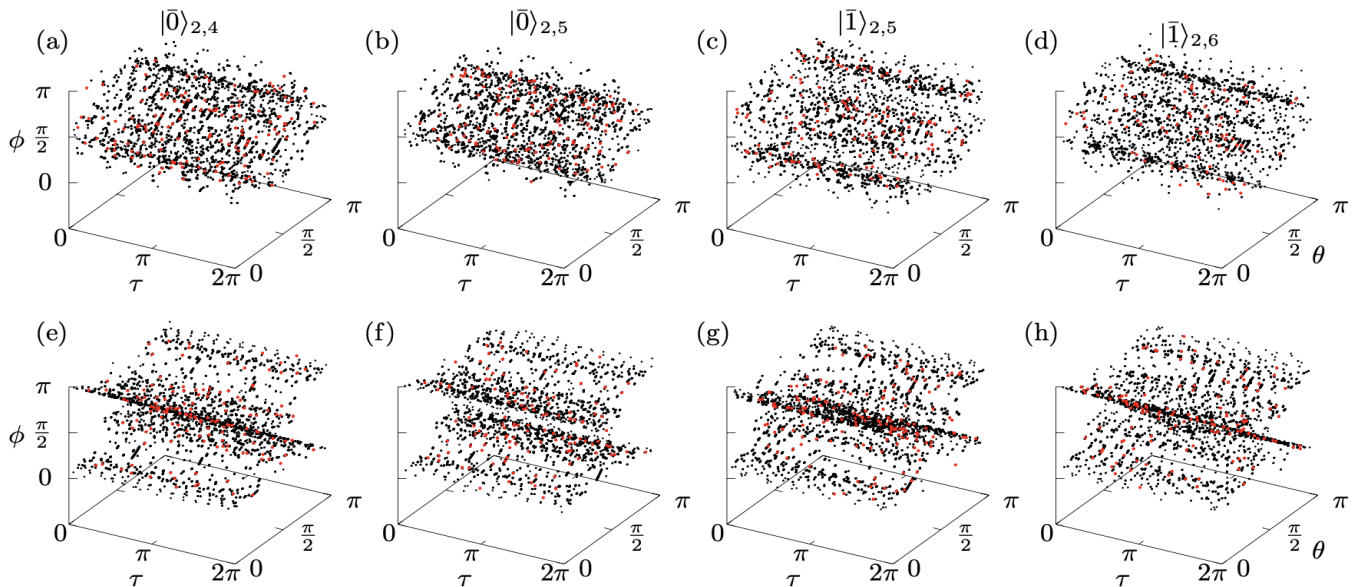


Figure 5. Combinations of  $\{\tau, \theta, \phi\}$  for which the fidelity ( $F_{2e_{\pm}}$  in Eq. (22)) of the postselected oscillator state in Eq. (21) reaches unity (within numerical precision) with each of the four three-component binomial targets  $|\bar{0}\rangle_{2,4}$ ,  $|\bar{0}\rangle_{2,5}$ ,  $|\bar{1}\rangle_{2,5}$ , and  $|\bar{1}\rangle_{2,6}$  are shown. As in Fig. 4, the top row corresponds to the case  $n_2 = n_1 + m$  ( $F_{2e_+}$ ), while the bottom row corresponds to  $n_2 = n_1 - m$  ( $F_{2e_-}$ ). All sampling details and fidelity thresholds are identical to those used in Fig. 4.

jected onto a four-Fock superposition state given by

$$|\psi_o(\tau)\rangle_{4e} = \mathcal{N}_{4e} \{ x_2(\tau) |n_1\rangle + x_4(\tau) |n_1 - m\rangle + y_2(\tau) |n_2\rangle + y_4(\tau) |n_2 - m\rangle \}, \quad (20)$$

where  $\mathcal{N}_{4e}$  is the normalization factor.

Following the same analysis as for the ground-state projection, the accessible Fock ladders again fall into two cases. For  $n_2 = n_1 + m$ , the relevant oscillator subspace is  $k_0, k_1, k_2 = n_1 - m, n_1, n_1 + m$ ; for  $n_2 = n_1 - m$ , it is  $k_0, k_1, k_2 = n_1 - 2m, n_1 - m, n_1$ . In analogy with the earlier analysis, the postselected state arising in both cases assumes the unified form

$$|\psi_o(\tau)\rangle_{3e_{\pm}} = \mathcal{N}_{3e_{\pm}} \sum_{l=0}^2 C_{le}^{(\pm)}(\tau, \theta, \phi) |k_l\rangle, \quad (21)$$

where the exact expressions of the coefficients are once again tabulated in Table III. The normalization  $\mathcal{N}_{3e_{\pm}} = \left\{ |C_{0e}^{(\pm)}|^2 + |C_{1e}^{(\pm)}|^2 + |C_{2e}^{(\pm)}|^2 \right\}^{-1/2}$ .

As before, by expressing each of the sixteen target states in the generic form  $\sum_l c_l |k_l\rangle$ , the fidelity for both constructions can be written compactly as

$$F_{3e_{\pm}}(\tau, \theta, \phi) = \frac{\left| \sum_{l=0}^2 c_l C_{le}^{(\pm)}(\tau, \theta, \phi) \right|^2}{\sum_{k=0}^2 \left| C_{le}^{(\pm)}(\tau, \theta, \phi) \right|^2}. \quad (22)$$

We again perform a numerical optimization over the control parameters  $\theta$ ,  $\phi$ , and  $\tau$  across the same ranges

Table V. Counts of parameter triplets  $(\tau, \theta, \phi)$  for which the fidelity  $F_{3e_{\pm}}$  (see Eq. (22)) between the engineered three-Fock-component state in Eq. (21) and the corresponding sixteen target codeword satisfies  $|F_{3e_{\pm}} - 1| \leq 10^{-4}$  or  $10^{-6}$ . The remaining details are identical to those in Table IV.

State	$n_2 = n_1 + m$		State	$n_2 = n_1 - m$	
	$N_{10^{-4}}$	$N_{10^{-6}}$		$N_{10^{-4}}$	$N_{10^{-6}}$
$ \bar{0}\rangle_{2,4}$	14809	159	$ \bar{0}\rangle_{2,4}$	13224	146
$ \bar{0}\rangle_{2,5}$	13311	131	$ \bar{0}\rangle_{2,5}$	12496	133
$ \bar{1}\rangle_{2,5}$	13601	139	$ \bar{1}\rangle_{2,5}$	16357	170
$ \bar{1}\rangle_{2,6}$	10752	89	$ \bar{1}\rangle_{2,6}$	13587	150

as in the previous analysis, and find that many parameter combinations yield unit fidelity. The corresponding scatter plots are shown in Fig. 5, further illustrating the substantial flexibility available when synthesizing the target code states in this setting. A summary of the fidelity counts is provided in Table V. Although the optimal parameter sets appear sparse in Figs. 2–5, their finite clustering demonstrates that the protocol tolerates small deviations in the control parameters, indicating robustness against moderate experimental imperfections in  $\tau$ ,  $\theta$ , and  $\phi$ .

Before proceeding, we note that this procedure can be systematically extended to generate larger superpositions involving four or more Fock states. In principle, the four-component Fock states can be readily realized from Eqs. (17) and (20) by selecting suitable values of  $n_1$ ,  $n_2$ ,  $m$  and subsequently optimizing the control parameters. An explicit example for a four-component state

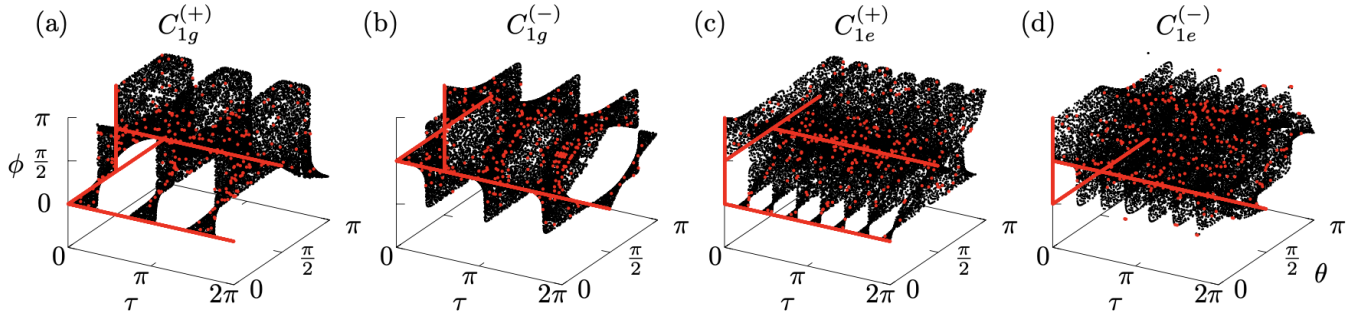


Figure 6. Combinations of  $\{\tau, \theta, \phi\}$  for which the functions  $C_{1g}^{(\pm)}$  and  $C_{1e}^{(\pm)}$  defined in Table III vanish. Numerical sampling was performed over 1001 values of  $\tau$  in the range  $[0, 2\pi]$  and 501 values each for  $\theta$  and  $\phi$  in  $[0, \pi]$ . All displayed points satisfy a numerical tolerance of  $\leq 10^{-4}$ , while red points highlight those meeting a stricter threshold of  $\leq 10^{-6}$ .

is provided in Appendix A. Importantly, as the number of target Fock components increases further, the number of required MPJC interaction steps grows accordingly, leading to a corresponding increase in the computational overhead for numerical optimization.

## VI. REDUCING ORDER OF MULTIPHOTON INTERACTIONS

Thus far, in engineering binomial code states, we have observed that increasing the number of correctable losses ( $L$ ) necessitates a corresponding increase in the value of  $m$ . As a result, generating code states with large  $L$  rapidly becomes practically infeasible. In this section, we address this limitation and demonstrate that the required  $m$  can, in fact, be reduced by a factor of two when the code states are superpositions of two Fock states. This comes at the cost of increasing the number of times the MPJC interaction needs to be implemented.

Recall that a single MPJC step produces superpositions of  $|n_1\rangle$  and  $|n_1 + m\rangle$  (or  $|n_1\rangle$  and  $|n_1 - m\rangle$ ) upon postselecting the qubit in the ground (or excited) state (see Eqs. (8) and (10)). Alternatively, one can employ the three-Fock superposition states  $|\psi_o(\tau)\rangle_{3g\pm}$  and  $|\psi_o(\tau)\rangle_{3e\pm}$  (Eqs. (18) and (21)) and eliminate the intermediate Fock components  $C_{1g}^{(\pm)}$  or  $C_{1e}^{(\pm)}$  by appropriately tuning the three control parameters  $\theta$ ,  $\phi$ , and  $\tau$ . This procedure yields superpositions of  $|n_1\rangle$  and  $|n_1 + 2m\rangle$  for  $|\psi_o(\tau)\rangle_{3g+}$ , superpositions of  $|n_1 - m\rangle$  and  $|n_1 + m\rangle$  for  $|\psi_o(\tau)\rangle_{3g-}$  and  $|\psi_o(\tau)\rangle_{3e+}$ , and superpositions of  $|n_1\rangle$  and  $|n_1 - 2m\rangle$  for  $|\psi_o(\tau)\rangle_{3e-}$ . In each case, this effectively doubles the separation between the Fock components while keeping the MPJC interaction order fixed.

In general, the superposition coefficients produced by the MPJC protocol need not coincide exactly with those of the target binomial codeword. In such cases, the intermediate oscillator state can, in principle, be deterministically mapped onto the desired code state by applying a suitable bosonic unitary acting within the relevant finite-dimensional Fock subspace. These uni-

tarities include number-selective phase operations (SNAP gates) and their generalizations, which provide full controllability over amplitudes and phases within a chosen Fock manifold and have been extensively demonstrated in circuit- and cavity-QED platforms [84]. We therefore treat this final single-mode operation as a controllable post-processing step and focus below on a representative example illustrating the procedure.

Consider the binomial state  $|\bar{0}\rangle_{2,2} = (|0\rangle + |4\rangle)/\sqrt{2}$ . In the one-step MPJC protocol, generating this state requires a multiphoton order  $m = 4$ . Using the two-step protocol, however, the same state can be realized with a reduced multiphoton order  $m = 2$ . To obtain this target from  $|\psi_o(\tau)\rangle_{3g+}$ , it suffices to set  $n_1 = 0$ ; for  $|\psi_o(\tau)\rangle_{3g-}$  or  $|\psi_o(\tau)\rangle_{3e+}$ , one should set  $n_1 = 2$ ; and for  $|\psi_o(\tau)\rangle_{3e-}$ ,  $n_1 = 4$ . Substituting the corresponding  $n_1$  and  $m$  values into Eqs. (18) and (21) produces oscillator states that are superpositions of  $|0\rangle$ ,  $|2\rangle$ , and  $|4\rangle$ . The coefficient of the intermediate Fock state  $|2\rangle$  in each case is given by

$$C_{1g}^{(+)} = \cos \theta \sin \phi \cos \tau_g - \sin \theta \cos \phi \sin \tau_g, \quad (23a)$$

$$C_{1g}^{(-)} = \cos \theta \cos \phi \cos \tau_g - \sin \theta \sin \phi \sin \tau_g, \quad (23b)$$

$$C_{1e}^{(+)} = \sin \theta \cos \phi \cos \tau_e + \cos \theta \sin \phi \sin \tau_e, \quad (23c)$$

$$C_{1e}^{(-)} = \cos \theta \cos \phi \sin \tau_e + \sin \theta \sin \phi \cos \tau_e, \quad (23d)$$

where  $\tau_g = \sqrt{2}\tau$  and  $\tau_e = \sqrt{12}\tau$ . The next step is to numerically optimize the control parameters  $(\theta, \phi, \tau)$  so that these coefficients vanish up to a desired numerical precision.

The resulting optimal parameter combinations, for which  $C_{1g}^{(\pm)}$  and  $C_{1e}^{(\pm)}$  vanish within a tolerance of  $10^{-4}$ , are shown as scatter plots in Fig. 6. A large number of valid solutions highlight the flexibility of the protocol. Selecting any such combination yields oscillator states of the form  $\alpha|0\rangle + \beta|4\rangle$ . If one of the resulting amplitude combinations  $(\alpha, \beta)$  does not match the target values, a final unitary operation needs to be applied to transform the intermediate state into the desired binomial state with high fidelity.

Before proceeding, we emphasize that the scheme de-

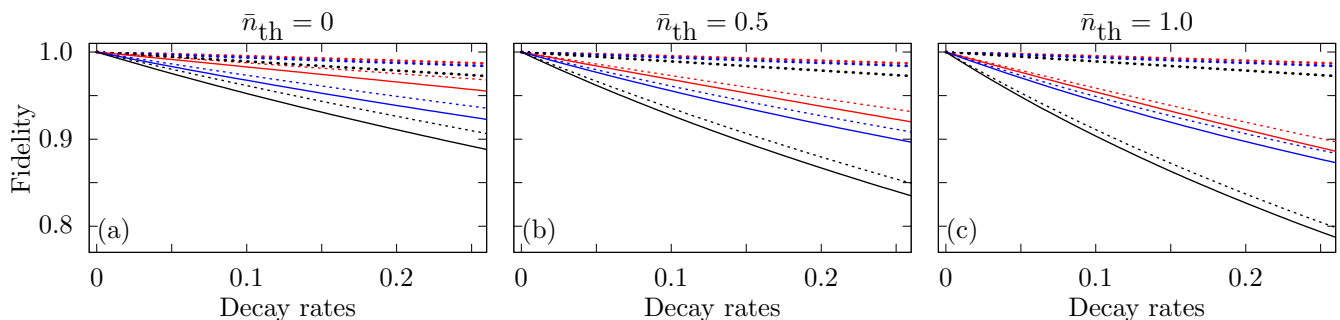


Figure 7. Fidelity degradation of the logical state  $|\bar{0}\rangle_{2,2}$  as a function of the decay rates, under the influence of system–environment interactions. Panels (a)–(c) correspond to increasing thermal bath occupations  $\bar{n}_{\text{th}}$ , as indicated above each panel. The values of  $\theta$  and  $\tau$  are fixed to those for which the fidelity first reaches unity (within a numerical precision of  $10^{-6}$ ) in the ideal, dissipation-free case. Three dissipation scenarios are considered: (i) oscillator-only coupling (red), (ii) qubit-only coupling (blue), and (iii) joint coupling of both subsystems to a common bath (black). In each case, dashed and dotted lines denote the effects of pure dissipation and pure dephasing, respectively, while solid lines represent the combined influence of both channels.

scribed in this section applies exclusively to code states comprising superpositions of two Fock states. Moreover, the reduction in the required  $m$  value by a factor of two is a one-time improvement; further reductions by factors of 4, 8, and so on are not supported within this approach.

## VII. ENVIRONMENTAL EFFECTS

Until now, our analysis has focused exclusively on ideal unitary evolution of the bipartite quantum system, neglecting the critical effects of system–environment interactions. In this section, we extend the study to include these effects by numerically simulating the full open-system state-preparation dynamics. Specifically, we replace the unitary MPJC evolution with a Lindblad master equation that accounts for both qubit relaxation and oscillator photon loss, such that the codeword is generated during the dissipative evolution rather than being prepared unitarily and subsequently propagated under dissipation. We adopt the standard Lindblad formalism, which relies on the Markovian approximation and other common assumptions such as the Born and secular approximations. Within this framework, the evolution of the reduced density matrix of the bipartite system,  $\rho_S(t)$ , is governed by the Lindblad master equation

$$\frac{d\rho_S}{dt} = -i[H, \rho_S] + \sum_k \left( L_k \rho_S L_k^\dagger - \frac{1}{2} [\rho_S, L_k^\dagger L_k] \right). \quad (24)$$

Here,  $L_k = \sqrt{\lambda_k} A_k$  are the collapse (Lindblad) operators, where the environment couples to the system through operators  $A_k$  with corresponding rates  $\lambda_k$ . To simplify the numerical analysis, we assume that both the oscillator and the two-level system interact with a common thermal environment at a temperature characterized by the mean thermal occupation  $\bar{n}_{\text{th}}$ .

For the bosonic mode, the relevant Lindblad operators are  $\sqrt{\lambda_{os_r}(1 + \bar{n}_{\text{th}})} a$ ,  $\sqrt{\lambda_{os_a} \bar{n}_{\text{th}}} a^\dagger$ , and  $\sqrt{\lambda_{os_d}} a^\dagger a$  which lead to emission/relaxation, absorption, and dephasing effects, respectively. Similarly, for the two-level system, the corresponding Lindblad operators are  $\sqrt{\lambda_{qb_r}(1 + \bar{n}_{\text{th}})} \sigma_-$ ,  $\sqrt{\lambda_{qb_a} \bar{n}_{\text{th}}} \sigma_+$ , and  $\sqrt{\lambda_{qb_d}} \sigma_z$ . While both relaxation and absorption rates depend on the bath temperature  $\bar{n}_{\text{th}}$ , the dephasing rates are temperature-independent. For simplicity, we assume  $\lambda_{os_r} = \lambda_{os_a}$ , and  $\lambda_{qb_r} = \lambda_{qb_a}$ .

The control parameters ( $\theta$ ,  $\phi$ ,  $\tau$ ) used in the open-system simulations are taken from the unitary optimization discussed in Secs. III–VI. Although these parameters are not re-optimized in the presence of dissipation, they provide a physically meaningful baseline for assessing how environmental decoherence degrades the performance of the protocol relative to the ideal unitary case.

To illustrate the impact of system–environment interactions on state preparation, we consider a representative example: the logical codeword  $|\bar{0}\rangle_{2,2}$ . While our analysis focuses on this specific case, we have verified that qualitatively similar behavior is observed for other logical states constructed as superpositions of two Fock states. To streamline the analysis and mitigate the effects of decoherence, we fix the parameter  $\theta$  to the value at which the fidelity first reaches unity (within a numerical threshold of  $10^{-6}$ ) in the absence of dissipation. This choice minimizes additional infidelity arising from the interaction with the environment. For the state  $|\bar{0}\rangle_{2,2}$ , we find numerically that this occurs at  $\tau = 0.037699$  with the corresponding  $\theta = 1.432566$ .

We first consider the case of zero temperature ( $\bar{n}_{\text{th}} = 0$ ), where decoherence arises exclusively from vacuum fluctuations—i.e., energy relaxation and dephasing in the absence of thermal excitations [see Fig. 7(a)]. The relevant collapse operators governing the open-system dynamics are  $\sqrt{\lambda_{os_r}} a$  and  $\sqrt{\lambda_{os_d}} a^\dagger a$  for the oscillator, and  $\sqrt{\lambda_{qb_r}} \sigma_-$  and  $\sqrt{\lambda_{qb_d}} \sigma_z$  for the qubit. We analyze three distinct scenarios: (i) the oscillator is coupled to the en-

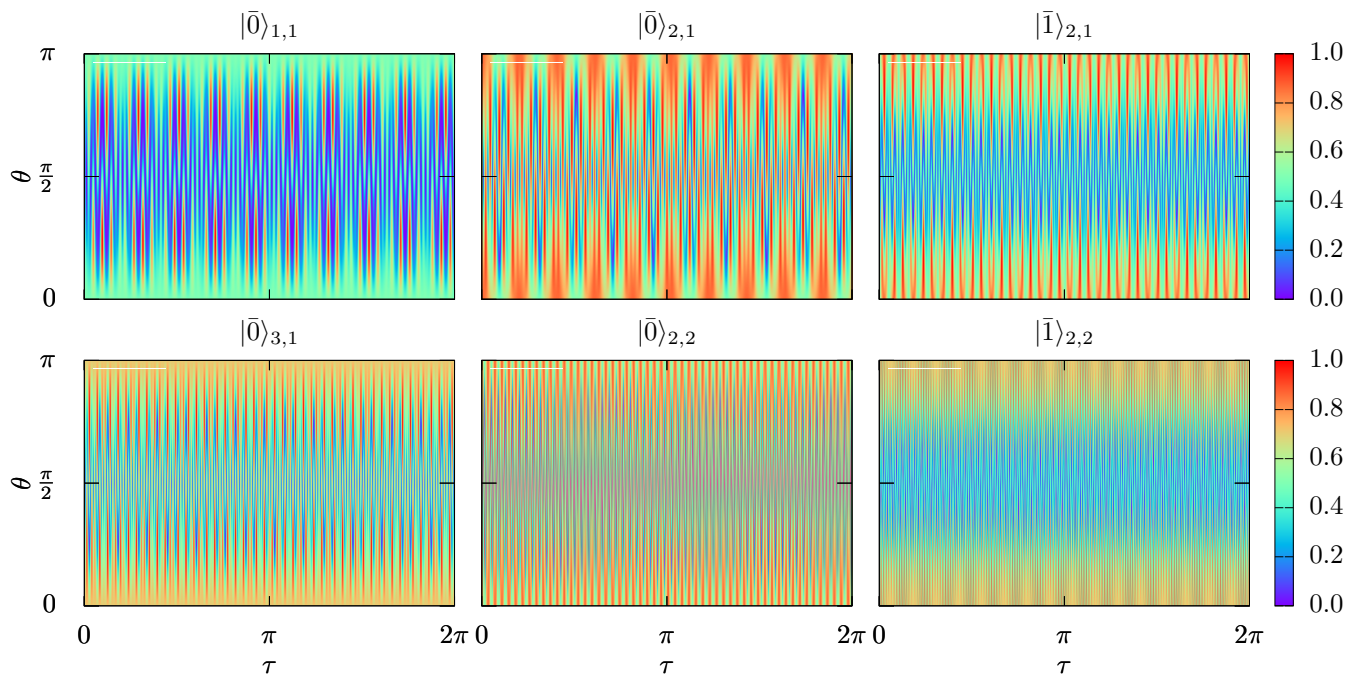


Figure 8. Fidelity between the time-evolved oscillator state  $\rho_o(\tau)$  [as given in Eq. (25)] and the corresponding target binomial codewords  $|\bar{0}\rangle_{1,1}$ ,  $|\bar{0}\rangle_{2,1}$ ,  $|\bar{1}\rangle_{2,1}$ ,  $|\bar{0}\rangle_{3,1}$ ,  $|\bar{0}\rangle_{2,2}$ , and  $|\bar{1}\rangle_{2,2}$ , plotted as a function of the evolution time  $\tau$  and the qubit superposition angle  $\theta$ . In contrast to the probabilistic protocol, no pair of  $(\tau, \theta)$  achieves unit fidelity within a numerical tolerance of  $10^{-4}$ , highlighting the constrained parameter space inherent in the deterministic generation scheme (see main text).

environment (red curves), (ii) the qubit is coupled (blue curves), and (iii) both subsystems are coupled simultaneously (black curves). In all cases, dashed and dotted lines correspond to pure dissipation and pure dephasing, respectively, while solid lines represent the combined influence of both. Notably, dephasing alone leads to a much lesser fidelity loss than energy relaxation for equivalent rates. Furthermore, the fidelity is more severely degraded when the qubit is coupled to the bath, as compared to the case in which the oscillator only interacts with the environment.

The effect of finite thermal excitations ( $\bar{n}_{\text{th}} > 0$ ) is illustrated in Figs. 7(b) and 7(c), where all relevant Lindblad operators actively contribute to the system's open dynamics. As expected, the pure dephasing curves remain identical across panels, reflecting their insensitivity to thermal excitations. In contrast, increasing the thermal occupation number  $\bar{n}_{\text{th}}$  leads to a progressive reduction in fidelity for all remaining cases, underscoring the detrimental role of thermal noise on the robustness of the encoded state.

For code states involving superpositions of a larger number of Fock states, the detrimental impact of losses is expected to be more pronounced. This is due to the fact that generating such states requires multiple sequential implementations of the MPJC interaction, with each stage introducing additional exposure to decoherence. As a result, losses compound over the course of the protocol, leading to a cumulative degradation in fidelity. However,

by carefully selecting an optimal interaction time at each step—preferably at the earliest instance when high fidelity is achieved—the effects of losses can be mitigated to a certain extent.

### VIII. DETERMINISTIC GENERATION OF BINOMIAL CODE STATES

In this section, we present the deterministic state-generation protocol, focusing on the two- and three-Fock-component states. In this protocol, instead of performing a projective measurement on the qubit, the oscillator state is obtained by tracing out the qubit subsystem from the joint system state. This operation inevitably reduces the purity of the oscillator state due to the loss of coherence arising from qubit-oscillator entanglement.

For the state  $|\Psi(\tau)\rangle$  in Eq.(5), the reduced density matrix of the oscillator, expressed in the truncated Fock basis  $|n_1 - m\rangle, |n_1\rangle, |n_1 + m\rangle$ , takes the form

$$\rho_o(\tau) = \begin{pmatrix} |x_4|^2 & x_2 x_4^* & x_1 x_3^* \\ x_2^* x_4 & |x_1|^2 + |x_2|^2 & 0 \\ x_1^* x_3 & 0 & |x_3|^2 \end{pmatrix}. \quad (25)$$

A particularly favorable condition for deterministic generation occurs at specific combinations of the evolution time  $\tau$  and the qubit superposition angle  $\theta$  for which the amplitudes  $|x_1| \approx 0$  and  $|x_3| \approx 0$ . Under these conditions, the reduced oscillator state approximates a nearly

Table VI. Optimal values of the parameters  $\theta_{\text{opt}}$  and  $\tau_{\text{opt}}$  at which each corresponding binomial code state achieves maximum fidelity in the deterministic generation protocol.

State	$\theta_{\text{opt}}$	$\tau_{\text{opt}}$	Max. Fidelity
$ \bar{0}\rangle_{2,2}$	2.356194	3.524866	0.998582
$ \bar{0}\rangle_{2,3}$	1.049291	5.441238	0.999613
$ \bar{1}\rangle_{2,3}$	2.620088	3.229557	0.999473
$ \bar{0}\rangle_{2,4}$	2.356194	3.229557	0.999052
$ \bar{0}\rangle_{3,3}$	2.092300	4.856902	0.999700
$ \bar{1}\rangle_{3,3}$	0.521504	0.772831	0.999763

Table VII. Optimal values of the parameters  $\theta_{\text{opt}}, \phi_{\text{opt}}$ , and  $\tau_{\text{opt}}$  at which each corresponding binomial code state achieves maximum fidelity in the deterministic generation protocol.

State	$\theta_{\text{opt}}$	$\phi_{\text{opt}}$	$\tau_{\text{opt}}$	Max. Fidelity
$ \bar{0}\rangle_{2,4}$	0.314159	1.897522	4.787787	0.991509
$ \bar{0}\rangle_{2,5}$	0.502655	1.771858	6.170088	0.978205
$ \bar{1}\rangle_{2,5}$	2.965663	0.967611	5.554336	0.987996
$ \bar{1}\rangle_{2,6}$	2.827433	1.244071	5.554336	0.950207

pure state of the form

$$|\psi_o(\tau)\rangle \approx x_4(\tau) |n_1 - m\rangle + x_2(\tau) |n_1\rangle, \quad (26)$$

which can be directly mapped (up to a local unitary transformation on the oscillator) to a binomial codeword comprising a superposition of two Fock states by selecting appropriate values of  $n_1$  and  $m$ , analogous to the probabilistic protocol. The task then reduces to identifying specific pairs of  $\tau$  and  $\theta$  that, under the constraint  $|x_1(\tau)| \approx 0$  and  $|x_3(\tau)| \approx 0$ , yield the desired superposition with high fidelity.

$$\rho_o(\tau) = \begin{pmatrix} |x_4|^2 & (x_2 + y_4)x_4^* & x_4^*y_2 & 0 \\ (x_2^* + y_4^*)x_4 & |x_1|^2 + |x_2 + y_4|^2 & x_1^*(x_3 + y_1) + (x_2^* + y_4^*)y_2 & x_1y_3^* \\ x_4^*y_2 & x_1(x_3^* + y_1^*) + (x_2 + y_4)y_2^* & |x_3 + y_1|^2 + |y_2|^2 & (x_3^* + y_1^*)y_3 \\ 0 & x_1^*y_3 & (x_3^* + y_1^*)y_3 & |y_3|^2 \end{pmatrix}. \quad (28)$$

Now, in the limit,  $x_1 \approx 0$ ,  $x_3 \approx 0$ ,  $y_1(\tau) \approx 0$ ,  $y_3(\tau) \approx 0$ , the above density matrix assumes the pure state of the form

$$|\psi_o(\tau)\rangle \approx x_4 |n_1 - m\rangle + (x_2 + y_4) |n_1\rangle + y_2 |n_1 + m\rangle. \quad (29)$$

As before, this state can be mapped (up to a local unitary transformation on the oscillator) to a binomial codeword comprising a superposition of three Fock states by appropriately choosing the values of  $n_1$  and  $m$ . However, due to constraints on the coefficients, it is not possible to attain near-unity fidelity for the desired code states.

This constraint fundamentally distinguishes the deterministic protocol from its probabilistic counterpart. In the probabilistic approach,  $\tau$  and  $\theta$  are unconstrained and can be freely optimized to maximize the fidelity, allowing for a broader parameter search space. In contrast, the deterministic method limits the viable parameter sets, which inevitably reduces the achievable fidelity due to this restricted optimization landscape (see Fig. 8). This trade-off is clearly manifested in our numerical analysis, where no combination of  $(\tau, \theta)$  was found to yield unit fidelity (within a numerical threshold of  $10^{-4}$ ) for any of the six representative code states. The highest fidelities achieved in each case, along with the corresponding optimal parameter values, are summarized in Table VI. It is important to note that these results pertain to the idealized, closed-system implementation of the deterministic protocol and do not include the effects of system–environment interactions. As expected, numerical simulations confirm that the inclusion of such interactions leads to a further degradation in fidelity.

Continuing to the case of three-component Fock superpositions, we proceed by setting  $n_2 = n_1 + m$  in Eq. (15), which yields the following bipartite state

$$|\Psi(\tau)\rangle = x_1 |g, n_1\rangle + (x_2 + y_4) |e, n_1\rangle \\ + (x_3 + y_1) |g, n_1 + m\rangle + y_2 |e, n_1 + m\rangle \\ + x_4 |e, n_1 - m\rangle + y_3 |g, n_1 + 2m\rangle. \quad (27)$$

After tracing out the qubit subsystem from  $|\Psi(\tau)\rangle$  in Eq.(15), the reduced density matrix of the oscillator  $\rho_o(\tau)$ , can be expressed in the truncated Fock basis  $|n_1 - m\rangle, |n_1\rangle, |n_1 + m\rangle, |n_1 + 2m\rangle$ . It is given by

Representative best-case scenarios for the four states considered in this study are summarized in Table VII.

## IX. CONCLUDING REMARKS

Rotation-symmetric bosonic codes (RSBCs) encode quantum information in states invariant under discrete phase-space rotations, leveraging rotation symmetries to enhance error resilience and fault tolerance [14, 69, 85]. Various families of RSBCs have been proposed, including (squeezed) cat codes [30–33, 86, 87], Pegg–Barnett

codes [25], GKP-like codes [10, 23], and binomial codes [10, 48]. In this work, we focus on the binomial code family, which consists of finite superpositions of Fock states with coefficients drawn from a binomial distribution.

We have presented a general and high-fidelity scheme for synthesizing *arbitrary* binomial codewords by harnessing nonlinear multiphoton interactions between a bosonic mode (oscillator) and a two-level system (qubit). Our approach is based on the coherent dynamics of the multiphoton Jaynes–Cummings (MPJC) Hamiltonian and assumes experimentally reasonable capabilities: initialization of the oscillator and qubit, access to multiphoton interactions, and qubit measurements during the evolution. While iterative methods based on standard cavity QED interactions have proven effective for generating cat codes starting from easily prepared coherent states, a similar strategy is less practical for binomial codes. As discussed in Appendix C, the primitive states required for binomial codewords are themselves complex superpositions of Fock states and do not offer a clear experimental advantage over direct codeword generation.

A key insight from our analysis is the essential role of a coherent initial qubit state in generating superpositions of target Fock states. This requirement stems from the inability of the MPJC Hamiltonian to induce coherence in either subsystem if the joint initial state lacks it—a constraint highlighted in recent studies [63, 79]. More broadly, the challenge of harnessing noisy or incoherent resources for generating entanglement and coherence remains an active area of investigation [88–90]. This raises an important question: can the inclusion of an additional dispersive spin-boson interaction compensate for the coherence shortfall of MPJC dynamics and enable high-fidelity synthesis of bosonic code states using noisy initial resources? The authors aim to address this issue in the future.

Another important feature in our scheme is the ability to reduce the required multiphoton transition order by a factor of two without sacrificing fidelity, thus significantly enhancing the experimental feasibility of the protocol. This one-time improvement is achieved by judiciously selecting the initial oscillator state and exploiting coherent interference effects.

In developing our protocol, we explored two complementary approaches to generating binomial codewords. The probabilistic protocol, which relies on projective measurement of the qubit after joint evolution, offers higher fidelities and greater flexibility in scanning the parameter space, making it better suited for precise codeword synthesis. In contrast, the deterministic protocol, which involves tracing out the qubit degrees of freedom without any measurement, is operationally simpler and potentially more suitable in scenarios where projective measurements are inefficient, technically challenging, or resource-intensive. Due to the constrained parameter space accessible in the deterministic setting, this protocol typically achieves slightly lower fidelities.

Our results contribute to the broader effort of realizing fault-tolerant bosonic quantum computing, not only by identifying an efficient method for preparing logical codewords, but also by highlighting the utility of nonlinear light–matter interactions in continuous-variable quantum systems. The methods outlined here are versatile and can be extended to prepare larger classes of bosonic codewords, potentially including cat codes and other non-Gaussian encodings.

In summary, this work provides a scalable and practical pathway toward high-fidelity generation of binomial code states, addressing a critical bottleneck in the realization of bosonic quantum error correction.

## ACKNOWLEDGMENTS

We thank P. A. Ameen Yasir and S. Siddardha Cheluri for valuable discussions. We acknowledge funding from the BMBF/BMFTR in Germany (QR.X/QR.N, PhotonQ, QuKuK, QuaPhySI), from the Deutsche Forschungsgemeinschaft (DFG, German Research Foundation) – Project-ID 429529648 – TRR 306 QuCoLiMa (Quantum Cooperativity of Light and Matter), and also from the EU project CLUSTEC (Grant Agreement No. 101080173).

## Appendix A: Details on the state vector

In this Appendix, we present additional details on the oscillator state vectors obtained through our protocol for generating binomial codewords involving superpositions of two and three Fock states. Furthermore, we extend our analysis to include a representative example of a superposition of four Fock states, illustrating the scalability of the protocol to more complex codewords.

### 1. Superposition of two Fock states

Applying the time-independent Schrödinger equation,  $i\frac{d}{dt}|\Psi(t)\rangle = H_{\text{int}}|\Psi(t)\rangle$ , with  $H_{\text{int}}$  and  $|\Psi(t)\rangle$  as defined in Eqs. (2) and (5), respectively, we get four time-dependent coefficients that obey the following coupled differential equations

$$\dot{x}_1(\tau) = -\sqrt{n_1!/(n_1 - m)!}x_4(\tau), \quad (\text{A1a})$$

$$\dot{x}_2(\tau) = \sqrt{(n_1 + m)!/n_1!}x_3(\tau), \quad (\text{A1b})$$

$$\dot{x}_3(\tau) = -\sqrt{(n_1 + m)!/n_1!}x_2(\tau), \quad (\text{A1c})$$

$$\dot{x}_4(\tau) = \sqrt{n_1!/(n_1 - m)!}x_1(\tau), \quad (\text{A1d})$$

for  $n_1 \geq m$ . If  $n_1 < m$ ,  $\dot{x}_1(\tau) = 0$  and  $\dot{x}_4(\tau) = 0$ . Note that  $\tau = gt$ . The initial condition in Eq. (4) implies  $x_1(0) = \cos\theta$ ,  $x_2(0) = \sin\theta$ , and  $x_3(0) = x_4(0) = 0$ .

Solving the coupled differential equations with these initial values yields explicit expressions for all four time-dependent coefficients. The resulting solutions are provided in Eq. (6) of the main text.

## 2. Superposition of three Fock states

Following the same procedure as outlined earlier, and using the state  $|\Psi(t)\rangle$  defined in Eq.(15), we obtain a set of eight coupled differential equations describing the system's time evolution. The first four equations are identical to the ones presented in Eq.(A1), while the remaining four are given by

$$\dot{y}_1(\tau) = -\sqrt{n_2!/(n_2-m)!} y_4(\tau), \quad (\text{A2a})$$

$$\dot{y}_2(\tau) = \sqrt{(n_2+m)!/n_2!} y_3(\tau), \quad (\text{A2b})$$

$$\dot{y}_3(\tau) = -\sqrt{(n_2+m)!/n_2!} y_2(\tau), \quad (\text{A2c})$$

$$\dot{y}_4(\tau) = \sqrt{n_2!/(n_2-m)!} y_1(\tau). \quad (\text{A2d})$$

The initial conditions are given by  $x_1(0) = \cos\theta \cos\phi$ ,  $x_2(0) = \sin\theta \cos\phi$ ,  $y_1(0) = \cos\theta \sin\phi$ , and  $y_2(0) = \sin\theta \sin\phi$ , with all other coefficients vanishing initially:  $x_3(0) = x_4(0) = y_3(0) = y_4(0) = 0$ . Solving the resulting set of coupled differential equations yields all the eight coefficients and are given in Eq. (16).

## 3. Superposition of four and higher Fock states

In the main text, we showed that binomial codewords composed of superpositions of two or three Fock states can be engineered by choosing an appropriate initial state, selecting the multiphoton order  $m$ , and optimizing the control parameters ( $\theta$ ,  $\phi$ , and  $\tau$ ). Here, we extend this construction to superpositions involving larger numbers of Fock components by systematically applying the same procedure.

First, consider binomial states composed of four Fock components. A simple algebraic count shows that there exist eleven logical  $|\bar{0}\rangle$  states (five for  $K=6$  and six for  $K=7$ ) and thirteen logical  $|\bar{1}\rangle$  states (six for  $K=7$  and seven for  $K=8$ ). The corresponding generic forms of these four-component logical states are

$$|\bar{0}\rangle_{N,6} = \frac{1}{4\sqrt{2}} (|0\rangle + \sqrt{15}|2N\rangle + \sqrt{15}|4N\rangle + |6N\rangle), \quad (\text{A3a})$$

$$|\bar{0}\rangle_{N,7} = \frac{1}{8} (|0\rangle + \sqrt{21}|2N\rangle + \sqrt{35}|4N\rangle + \sqrt{7}|6N\rangle), \quad (\text{A3b})$$

$$|\bar{1}\rangle_{N,7} = \frac{1}{8} (\sqrt{7}|N\rangle + \sqrt{35}|3N\rangle + \sqrt{21}|5N\rangle + |7N\rangle), \quad (\text{A3c})$$

$$|\bar{1}\rangle_{N,8} = \frac{1}{4} (|N\rangle + \sqrt{7}|3N\rangle + \sqrt{7}|5N\rangle + |7N\rangle). \quad (\text{A3d})$$

Direct generation of these four-Fock-component target binomial states from Eqs. (17) (ground-state postselection) and (20) (excited-state postselection) requires appropriate choices of  $n_1$ ,  $n_2$ , and  $m$ , as summarized in Table VIII. Note that for each logical state, two parameter combinations are possible; from an experimental standpoint, it is preferable to choose the combination with the smaller  $m$ . Once  $n_1$ ,  $n_2$ , and  $m$  are fixed, the next step is to identify the control parameters ( $\theta, \phi, \tau$ ) that maximize the fidelity to the target state. We performed this numerical search for two representative cases,  $|\bar{0}\rangle_{N,6}$  and  $|\bar{1}\rangle_{2,7}$ . Remarkably, for both states—and for all admissible choices of  $m$  and postselection—we found that only a small number of parameter triplets (between 4 and 26) achieve fidelity within a numerical tolerance of  $10^{-4}$ , and none met the stricter threshold of  $10^{-6}$ .

Table VIII. Parameter sets  $\{n_1, n_2, m\}$  for generating four-Fock-component logical states via Eqs. (17) (ground-state postselection) and (20) (excited-state postselection).

Postselection	Logical state	$n_1$	$n_2$	$m$
$ g\rangle$	$ \bar{0}\rangle$	0	4N	2N
		0	2N	4N
	$ \bar{1}\rangle$	N	5N	2N
		N	3N	4N
$ e\rangle$	$ \bar{0}\rangle$	2N	6N	2N
		4N	6N	4N
	$ \bar{1}\rangle$	3N	7N	2N
		5N	7N	4N

The limited number of viable parameter combinations for directly generating these four-component states can be mitigated by increasing the number of MPJC steps. To illustrate this, we begin by preparing the full system in the initial state

$$|\Psi(0)\rangle = (\cos\theta |g\rangle + \sin\theta |e\rangle) \otimes (\sin\phi_1 \cos\phi_2 |n_1\rangle + \sin\phi_1 \sin\phi_2 |n_2\rangle + \cos\phi_1 |n_3\rangle). \quad (\text{A4})$$

The time-evolved state in this case vector takes the form

$$|\Psi(\tau)\rangle = \sum_{i=1}^4 x_i(\tau) |\chi_i(n_1)\rangle + \sum_{i=1}^4 y_i(\tau) |\chi_i(n_2)\rangle + \sum_{i=1}^4 z_i(\tau) |\chi_i(n_3)\rangle, \quad (\text{A5})$$

where  $|\chi_i(n)\rangle \in \{|g, n\rangle, |e, n\rangle, |g, n+m\rangle, |e, n-m\rangle\}$ .

Proceeding as before, we now derive the set of twelve coupled differential equations governing the system dynamics. The initial conditions are given by  $x_1(0) = \cos\theta \sin\phi_1 \cos\phi_2$ ,  $x_2(0) = \sin\theta \sin\phi_1 \cos\phi_2$ ,  $y_1(0) = \cos\theta \sin\phi_1 \sin\phi_2$ ,  $y_2(0) = \sin\theta \sin\phi_1 \sin\phi_2$ ,  $z_1(0) = \cos\theta \cos\phi_1$ ,  $z_2(0) = \sin\theta \cos\phi_1$ , with all remaining coefficients initialized to zero:  $x_3(0) = x_4(0) = y_3(0) =$

$y_4(0) = z_3(0) = z_4(0) = 0$ . The time-dependent amplitudes factorize as

$$x_i(\tau) = \sin \phi_1 \cos \phi_2 x_i^{(2)}(n_1, m, \theta, \tau), \quad (\text{A6a})$$

$$y_i(\tau) = \sin \phi_1 \sin \phi_2 x_i^{(2)}(n_2, m, \theta, \tau), \quad (\text{A6b})$$

$$z_i(\tau) = \cos \phi_1 x_i^{(2)}(n_3, m, \theta, \tau), \quad (\text{A6c})$$

where  $x_i^{(2)}$  denotes the coefficients of the two-Fock solution given previously in Eq. (6). Thus the temporal evolution decomposes naturally into three independent excitation manifolds, weighted by  $\sin \phi_1 \cos \phi_2$ ,  $\sin \phi_1 \sin \phi_2$ , and  $\cos \phi_1$ , respectively. For  $n_1 < m$ ,  $x_1(\tau) = \cos \theta \sin \phi_1 \cos \phi_2$ ,  $x_4(\tau) = 0$ , for  $n_2 < m$ ,  $y_1(\tau) = \cos \theta \sin \phi_1 \sin \phi_2$ ,  $y_4(\tau) = 0$ , and for  $n_3 < m$ ,  $z_1(\tau) = \cos \theta \cos \phi_1$ ,  $z_4(\tau) = 0$ .

Next, subject to a projective qubit ground and excited state measurements, the (unnormalized) oscillator states reduces to

$$|\psi_o(\tau)\rangle_g = x_1 |n_1\rangle + x_3 |n_1 + m\rangle + y_1 |n_2\rangle + y_3 |n_2 + m\rangle + z_1 |n_3\rangle + z_3 |n_3 + m\rangle, \quad (\text{A7a})$$

$$|\psi_o(\tau)\rangle_e = x_2 |n_1\rangle + x_4 |n_1 - m\rangle + y_2 |n_2\rangle + y_4 |n_2 - m\rangle + z_2 |n_3\rangle + z_4 |n_3 - m\rangle. \quad (\text{A7b})$$

There are multiple ways in which the six-Fock-component superposition in Eq. (A7) can be reduced to four distinct components through appropriate choices of  $n_1$ ,  $n_2$ , and  $m$ . As an illustrative example, consider the logical state  $|\bar{0}\rangle_{2,6}$ . One possible realization from Eq. (A7b) is obtained by choosing  $n_1 = m = 4$ ,  $n_2 = 8$ , and  $n_3 = 12$ , which yields the following explicit form of the oscillator state

$$|\phi\rangle = \mathcal{N} (C_0 |0\rangle + C_1 |4\rangle + C_2 |8\rangle + C_3 |12\rangle), \quad (\text{A8})$$

where

$$C_0 = \cos \theta \sin \phi_1 \cos \phi_2 \sin \left( \sqrt{4!} \tau \right),$$

$$C_1 = \sin \theta \sin \phi_1 \cos \phi_2 \cos \left( \sqrt{8!/4!} \tau \right) + \cos \theta \sin \phi_1 \sin \phi_2 \sin \left( \sqrt{8!/4!} \tau \right), \quad (\text{A9})$$

$$C_2 = \sin \theta \sin \phi_1 \sin \phi_2 \cos \left( \sqrt{12!/8!} \tau \right) + \cos \theta \cos \phi_1 \sin \left( \sqrt{12!/8!} \tau \right), \quad (\text{A10})$$

$$C_3 = \sin \theta \cos \phi_1 \cos \left( \sqrt{16!/12!} \tau \right) \}, \quad (\text{A11})$$

and  $\mathcal{N}$  the normalization factor. The fidelity between the state  $|\phi\rangle$  and the target binomial codeword  $|\bar{0}\rangle_{2,6}$  is given by

$$F = \frac{\mathcal{N}^2}{32} \left| C_0 + \sqrt{15} C_1 + \sqrt{15} C_2 + C_3 \right|^2. \quad (\text{A12})$$

As in previous cases, achieving unit fidelity requires numerical optimization over the parameter  $\theta$ ,  $\phi_1$ ,  $\phi_2$ ,

and the evolution time  $\tau$ . Specifically, we scanned  $\theta$ ,  $\phi_1$ , and  $\phi_2$  over the interval  $[0, \pi]$  using 251 uniformly spaced points for each, and  $\tau$  over  $[0, 2\pi]$  with 501 points. Within this parameter space, we identified approximately 5024 parameter combinations for which the fidelity approaches unity to within a numerical precision of  $10^{-4}$ , and six combinations that satisfy a more stringent threshold of  $10^{-6}$ . This demonstrates a clear increase in the number of viable parameter choices, albeit at the cost of an additional MPJC step.

On the other hand, the six-Fock-component superposition state in Eq. (A7a) can be reduced to five distinct components in exactly six different ways, namely by choosing any of the constraints  $n_i = n_j \pm m$  where  $i \neq j$  and  $1 \leq i, j \leq 3$ .

In the case  $n_2 = n_1 + m$ , the accessible Fock ladder is  $k_0, k_1, k_2, k_3, k_4 = n_1, n_1 + m, n_1 + 2m, n_3, n_3 + m$ . For the alternative choice  $n_2 = n_1 - m$  with  $n_1 \geq m$ , the ladder becomes  $n_1 - m, n_1, n_1 + m, n_3, n_3 + m$ . In both cases, the oscillator state derived from Eq. (A7a) can be written in the unified form

$$|\psi_o(\tau)\rangle_{5g\pm} = \mathcal{N}_{5g\pm} \sum_{l=0}^4 C_{lg}^{(\pm)}(\tau, \theta, \phi_1, \phi_2) |k_l\rangle. \quad (\text{A13})$$

where  $\mathcal{N}_{5g\pm}$  is the normalization factor, and the exact expressions of the coefficients  $C_{lg}^{(\pm)}$  can be straightforwardly obtained. Writing the target states in the form  $\sum_l c_l |k_l\rangle$  for both cases, the fidelity for both constructions can be succinctly expressed in the form

$$F_{5g\pm}(\tau, \theta, \phi) = \frac{\left| \sum_{l=0}^4 c_l C_{lg}^{(\pm)}(\tau, \theta, \phi_1, \phi_2) \right|^2}{\sum_{l=0}^4 \left| C_{lg}^{(\pm)}(\tau, \theta, \phi_1, \phi_2) \right|^2}. \quad (\text{A14})$$

The next step is to scan over the control parameters  $(\theta, \phi_1, \phi_2, \tau)$  and identify combinations for which the fidelity reaches unity within the desired numerical precision. We also note that the state in Eq. (A5) can, in principle, be used directly to generate binomial code states comprising six Fock components. Although we do not present an explicit example here, such a construction is straightforward in principle; the only limitation is that the corresponding optimization becomes increasingly demanding as the number of control parameters grows.

## Appendix B: Controllability of two-Fock-state superpositions

In this Appendix, we show that the states

$$|\psi_o(\tau)\rangle_{2g} = \mathcal{N}_{2g} [\cos \theta |n_1\rangle - \sin \theta \sin(a_{n_1, m} \tau) |n_1 + m\rangle],$$

$$|\psi_o(\tau)\rangle_{2e} = \mathcal{N}_{2e} [\sin \theta \cos(a_{n_1, m} \tau) |n_1\rangle + \cos \theta \sin(b_{n_1, m} \tau) |n_1 - m\rangle],$$

enable arbitrary superpositions of the respective Fock-state pairs  $\{|n_1\rangle, |n_1 + m\rangle\}$  and  $\{|n_1\rangle, |n_1 - m\rangle\}$ . In each case, the engineered interaction couples only a two-dimensional subspace of the oscillator Hilbert space, resulting in Rabi-type dynamics with number-dependent couplings  $a_{n_1, m} = \sqrt{(n_1 + m)!/n_1!}$  and  $b_{n_1, m} = \sqrt{n_1!/(n_1 - m)!}$ .

For  $|\psi_o(\tau)\rangle_{2g}$ , the amplitude ratio is given by

$$\frac{C_{n_1+m}}{C_{n_1}} = -\tan\theta \sin(a_{n_1, m}\tau). \quad (\text{B1})$$

The above ratio can take any real value since  $\tan\theta$  spans  $(-\infty, \infty)$  and  $\sin(a_{n_1, m}\tau) \in [-1, 1]$ , meaning that any real superposition of the form  $C_1 |n_1\rangle + C_2 |n_1 + m\rangle$  is directly reachable. If one additionally wishes to control the relative phase between the two components, this can be achieved by adjusting the phase of the external drive, which provides independent complex phase control of the superposition.

Similarly, for  $|\psi_o(\tau)\rangle_{2e}$ , the ratio

$$\frac{C_{n_1-m}}{C_{n_1}} = \cot\theta \tan(b_{n_1, m}\tau), \quad (\text{B2})$$

again covering all real values. This guarantees access to all normalized states  $C_1 |n_1\rangle + C_2 |n_1 - m\rangle$ .

Therefore, by tuning  $\theta$  and  $\tau$ , both manifolds provide full Bloch-sphere controllability within their respective two-Fock-state subspaces, enabling the preparation of arbitrary superpositions.

We mention in passing that although the states  $|\psi_o(\tau)\rangle_{2g}$  and  $|\psi_o(\tau)\rangle_{2e}$  allow full controllability within their two-dimensional Fock subspaces, the specific parameters  $(\theta, \tau)$  for a target superposition typically require a numerical search. This is because the effective couplings  $a_{n_1, m}$  and  $b_{n_1, m}$  are generally irrational, preventing a simple analytical solution. Numerical optimization over  $\theta$  and  $\tau$  efficiently identifies the desired superposition with high fidelity.

### Appendix C: Binomial codewords via rotation of primitive states

Following the framework developed in Ref. [14], in this Appendix, we demonstrate explicitly how the logical binomial codewords defined in Eq. (1) can be obtained from a single *primitive state* using parity-selective rotations. This construction places the binomial code within the broader class of RSBCs and highlights the underlying discrete rotational symmetries that structure these codes.

#### 1. Construction of binomial codewords from a primitive state

We define the primitive state as a weighted superposition over Fock states spaced by  $(S + 1)$ , with weights

drawn from binomial coefficients

$$|\Theta\rangle_{N, K} = \frac{1}{\sqrt{2^{K-1}}} \sum_{k=0}^K \sqrt{\binom{K}{k}} |Nk\rangle. \quad (\text{C1})$$

This state includes all Fock components required to build both logical codewords  $|\bar{0}\rangle_{N, K}$  and  $|\bar{1}\rangle_{N, K}$ , since it contains both even and odd values of  $k$ .

To extract the individual logical codewords, we exploit the discrete rotation symmetry in Fock space using the operator

$$\hat{R}(\phi) = e^{i\phi\hat{n}}, \quad \hat{n} = \hat{a}^\dagger\hat{a}. \quad (\text{C2})$$

In particular, a rotation by  $\phi = \pi$  maps each Fock state as  $\hat{R}(\pi)|n\rangle = (-1)^n|n\rangle$ , thus separating the primitive state into parity components.

Define the logical codewords as

$$|\bar{0}\rangle_{N, K} = \mathcal{N}_0 \left( |\Theta\rangle_{N, K} + \hat{R}(\pi) |\Theta\rangle_{N, K} \right), \quad (\text{C3})$$

$$|\bar{1}\rangle_{N, K} = \mathcal{N}_1 \left( |\Theta\rangle_{N, K} - \hat{R}(\pi) |\Theta\rangle_{N, K} \right), \quad (\text{C4})$$

where  $\mathcal{N}_\mu$  are normalization constants ( $\mu = 0, 1$ ). These operations project onto even and odd values of  $k$ , respectively, thereby isolating the desired logical basis states.

This construction guarantees orthogonality of the logical states and yields the exact codeword forms prescribed by the binomial code definition.

#### 2. Example: binomial code for $N = 3, S = 3$

As an illustrative example, consider the case where  $N = 3$  and  $K = 3$ , leading to Fock spacings of 3. As defined in Eq. (7), the binomial codewords are:  $|\bar{0}\rangle_{3, 3} = \frac{1}{2}(|0\rangle + \sqrt{3}|6\rangle)$ ,  $|\bar{1}\rangle_{3, 3} = \frac{1}{2}(\sqrt{3}|3\rangle + |9\rangle)$ . The associated primitive state is:

$$|\Theta\rangle_{3, 3} = \frac{1}{2} \left( |0\rangle + \sqrt{3}|3\rangle + \sqrt{3}|6\rangle + |9\rangle \right). \quad (\text{C5})$$

Applying the parity-selective rotation  $\hat{R}(\pi)$ , we obtain

$$\hat{R}(\pi) |\Theta\rangle_{3, 3} = \frac{1}{2} \left( |0\rangle - \sqrt{3}|3\rangle + \sqrt{3}|6\rangle - |9\rangle \right). \quad (\text{C6})$$

Therefore, it is straightforward to extract the logical states as shown below

$$|\bar{0}\rangle_{3, 3} = \frac{1}{\sqrt{4}} \left( |\Theta\rangle_{3, 3} + \hat{R}(\pi) |\Theta\rangle_{3, 3} \right) = \frac{1}{2} \left( |0\rangle + \sqrt{3}|6\rangle \right), \quad (\text{C7})$$

$$|\bar{1}\rangle_{3, 3} = \frac{1}{\sqrt{4}} \left( |\Theta\rangle_{3, 3} - \hat{R}(\pi) |\Theta\rangle_{3, 3} \right) = \frac{1}{2} \left( \sqrt{3}|3\rangle + |9\rangle \right). \quad (\text{C8})$$

This confirms the validity of the rotational construction and demonstrates a clear, experimentally feasible path to generating binomial codewords from a single resource state.

### 3. Practical considerations

The rotation-based construction of binomial codewords from a primitive state provides a unified and elegant theoretical framework, highlighting the symmetry underlying these codes. However, from an experimental perspective, this approach does not necessarily reduce the complexity of state preparation. The primitive states  $|\Theta\rangle_{N,K}$  involve superpositions over all relevant Fock states  $Nk$  for  $k = 0, \dots, K$ , whereas the binomial codewords occupy only a parity-restricted subset of this space.

Preparing such primitive states requires coherent control over a larger number of Fock components, increasing the sensitivity to decoherence and operational infidelity. Although in principle these states can be generated using the same MPJC interactions that are used to synthesize

binomial codewords directly, doing so may be less efficient: if one already has access to controlled multiphoton interactions, generating the final codewords directly is typically more practical than preparing an intermediate superposition followed by rotation-based projections.

It is worth contrasting this with the family of cat codes, where the primitive state is a coherent state—a state that is straightforward to prepare experimentally with high fidelity. For cat codes, generating the entire family through rotations of this easily accessible primitive state is both conceptually elegant and experimentally practical [69]. In contrast, the more complex primitive states required for binomial codes limit the practical advantage of the rotational construction in actual implementations.

Thus, while the rotational construction offers valuable conceptual insight, it does not intrinsically simplify the experimental path to realizing binomial code states.

- 
- [1] Michael A. Nielsen and Isaac L. Chuang, *Quantum Computation and Quantum Information: 10th Anniversary Edition* (Cambridge University Press, 2010).
- [2] Simon J Devitt, William J Munro, and Kae Nemoto, “Quantum error correction for beginners,” *Rep. Prog. Phys.* **76**, 076001 (2013).
- [3] Barbara M. Terhal, “Quantum error correction for quantum memories,” *Rev. Mod. Phys.* **87**, 307–346 (2015).
- [4] Joschka Roffe, “Quantum error correction: an introductory guide,” *Contemp. Phys.* **60**, 226–245 (2019).
- [5] Adrian Cho, “The biggest flipping challenge in quantum computing,” *Science* **10**, 7332 (2020).
- [6] Samuel L. Braunstein and Peter van Loock, “Quantum information with continuous variables,” *Rev. Mod. Phys.* **77**, 513–577 (2005).
- [7] Christian Weedbrook, Stefano Pirandola, Raúl García-Patrón, Nicolas J. Cerf, Timothy C. Ralph, Jeffrey H. Shapiro, and Seth Lloyd, “Gaussian quantum information,” *Rev. Mod. Phys.* **84**, 621–669 (2012).
- [8] Alessio Serafini, *Quantum Continuous Variables* (CRC Press, 2017).
- [9] Samuel L. Braunstein, “Error correction for continuous quantum variables,” *Phys. Rev. Lett.* **80**, 4084–4087 (1998).
- [10] Victor V. Albert, Kyungjoo Noh, Kasper Duivenvoorden, Dylan J. Young, R. T. Brierley, Philip Reinhold, Christophe Vuillot, Linshu Li, Chao Shen, S. M. Girvin, Barbara M. Terhal, and Liang Jiang, “Performance and structure of single-mode bosonic codes,” *Phys. Rev. A* **97**, 032346 (2018).
- [11] C. Flühmann, T. L. Nguyen, M. Marinelli, V. Negnevitsky, K. Mehta, and J. P. Home, “Encoding a qubit in a trapped-ion mechanical oscillator,” *Nature* **566**, 513–517 (2019).
- [12] L. Hu, Y. Ma, W. Cai, X. Mu, Y. Xu, W. Wang, Y. Wu, H. Wang, Y. P. Song, C. L. Zou, S. M. Girvin, L.-M. Duan, and L. Sun, “Quantum error correction and universal gate set operation on a binomial bosonic logical qubit,” *Nat. Phys.* **15**, 503–508 (2019).
- [13] B M Terhal, J Conrad, and C Vuillot, “Towards scalable bosonic quantum error correction,” *Quantum Sci. Technol.* **5**, 043001 (2020).
- [14] Arne L. Grimsmo, Joshua Combes, and Ben Q. Baragiola, “Quantum computing with rotation-symmetric bosonic codes,” *Phys. Rev. X* **10**, 011058 (2020).
- [15] Weizhou Cai, Yuwei Ma, Weiting Wang, Chang-Ling Zou, and Luyan Sun, “Bosonic quantum error correction codes in superconducting quantum circuits,” *Fundamental Research* **1**, 50–67 (2021).
- [16] Atharv Joshi, Kyungjoo Noh, and Yvonne Y Gao, “Quantum information processing with bosonic qubits in circuit QED,” *Quantum Sci. Technol.* **6**, 033001 (2021).
- [17] Wen-Long Ma, Shruti Puri, Robert J. Schoelkopf, Michel H. Devoret, S.M. Girvin, and Liang Jiang, “Quantum control of bosonic modes with superconducting circuits,” *Science Bulletin* **66**, 1789–1805 (2021).
- [18] Brennan de Neeve, Thanh-Long Nguyen, Tanja Behrle, and Jonathan P. Home, “Error correction of a logical grid state qubit by dissipative pumping,” *Nat. Phys.* **18**, 296–300 (2022).
- [19] Zhaoyou Wang, Taha Rajabzadeh, Nathan Lee, and Amir H. Safavi-Naeini, “Automated discovery of autonomous quantum error correction schemes,” *PRX Quantum* **3**, 020302 (2022).
- [20] V. V. Sivak, A. Eickbusch, B. Royer, S. Singh, I. Tsioutsios, S. Ganjam, A. Miano, B. L. Brock, A. Z. Ding, L. Frunzio, S. M. Girvin, R. J. Schoelkopf, and M. H. Devoret, “Real-time quantum error correction beyond break-even,” *Nature* **616**, 50–55 (2023).
- [21] Anthony J. Brady, Alec Eickbusch, Shraddha Singh, Jing Wu, and Quntao Zhuang, “Advances in bosonic quantum error correction with Gottesman–Kitaev–Preskill codes: Theory, engineering and applications,” *Prog. Quantum Electron.* **93**, 100496 (2024).
- [22] Yijia Xu, Yixu Wang, Christophe Vuillot, and Victor V. Albert, “Letting the tiger out of its cage: Bosonic coding without concatenation,” *Phys. Rev. X* **15**, 041025 (2025).
- [23] Daniel Gottesman, Alexei Kitaev, and John Preskill, “Encoding a qubit in an oscillator,” *Phys. Rev. A* **64**, 012310 (2001).
- [24] Kyungjoo Noh, Victor V. Albert, and Liang Jiang, “Quantum capacity bounds of gaussian thermal loss

- channels and achievable rates with Gottesman-Kitaev-Preskill codes,” *IEEE Trans. Inf. Theory* **65**, 2563–2582 (2019).
- [25] Ben Q. Baragiola, Giacomo Pantaleoni, Rafael N. Alexander, Angela Karanjai, and Nicolas C. Menicucci, “All-gaussian universality and fault tolerance with the Gottesman-Kitaev-Preskill code,” *Phys. Rev. Lett.* **123**, 200502 (2019).
- [26] Kyungjoo Noh and Christopher Chamberland, “Fault-tolerant bosonic quantum error correction with the surface-Gottesman-Kitaev-Preskill code,” *Phys. Rev. A* **101**, 012316 (2020).
- [27] Kyungjoo Noh, Christopher Chamberland, and Fernando G.S.L. Brandão, “Low-overhead fault-tolerant quantum error correction with the surface-GKP code,” *PRX Quantum* **3**, 010315 (2022).
- [28] Jonathan Conrad, *The fabulous world of GKP codes*, Dissertation (2024).
- [29] P. T. Cochrane, G. J. Milburn, and W. J. Munro, “Macroscopically distinct quantum-superposition states as a bosonic code for amplitude damping,” *Phys. Rev. A* **59**, 2631–2634 (1999).
- [30] Zaki Leghtas, Gerhard Kirchmair, Brian Vlastakis, Robert J. Schoelkopf, Michel H. Devoret, and Mazyar Mirrahimi, “Hardware-efficient autonomous quantum memory protection,” *Phys. Rev. Lett.* **111**, 120501 (2013).
- [31] Mazyar Mirrahimi, Zaki Leghtas, Victor V Albert, Steven Touzard, Robert J Schoelkopf, Liang Jiang, and Michel H Devoret, “Dynamically protected cat-qubits: a new paradigm for universal quantum computation,” *New J. Phys.* **16**, 045014 (2014).
- [32] Marcel Bergmann and Peter van Loock, “Quantum error correction against photon loss using multicomponent cat states,” *Phys. Rev. A* **94**, 042332 (2016).
- [33] Linshu Li, Chang-Ling Zou, Victor V. Albert, Sreeraman Muralidharan, S. M. Girvin, and Liang Jiang, “Cat codes with optimal decoherence suppression for a lossy bosonic channel,” *Phys. Rev. Lett.* **119**, 030502 (2017).
- [34] Christopher Chamberland, Kyungjoo Noh, Patricio Arrangoiz-Arriola, Earl T. Campbell, Connor T. Hann, Joseph Iverson, Harald Putterman, Thomas C. Bohdanowicz, Steven T. Flammia, Andrew Keller, Gil Refael, John Preskill, Liang Jiang, Amir H. Safavi-Naeini, Oskar Painter, and Fernando G.S.L. Brandão, “Building a fault-tolerant quantum computer using concatenated cat codes,” *PRX Quantum* **3**, 010329 (2022).
- [35] Nissim Ofek, Andrei Petrenko, Reinier Heeres, Philip Reinhold, Zaki Leghtas, Brian Vlastakis, Yehan Liu, Luigi Frunzio, S. M. Girvin, L. Jiang, Mazyar Mirrahimi, M. H. Devoret, and R. J. Schoelkopf, “Extending the lifetime of a quantum bit with error correction in superconducting circuits,” *Nature* **536**, 441–445 (2016).
- [36] Reinier W. Heeres, Philip Reinhold, Nissim Ofek, Luigi Frunzio, Liang Jiang, Michel H. Devoret, and Robert J. Schoelkopf, “Implementing a universal gate set on a logical qubit encoded in an oscillator,” *Nat. Commun.* **8**, 94 (2017).
- [37] P. Campagne-Ibarcq, A. Eickbusch, S. Touzard, E. Zalgaller, N. E. Frattini, V. V. Sivak, P. Reinhold, S. Puri, S. Shankar, R. J. Schoelkopf, L. Frunzio, M. Mirrahimi, and M. H. Devoret, “Quantum error correction of a qubit encoded in grid states of an oscillator,” *Nature* **584**, 368–372 (2020).
- [38] Raphael Dahan, Gefen Baranes, Alexey Gorlach, Ron Ruimy, Nicholas Rivera, and Ido Kaminer, “Creation of optical cat and GKP states using shaped free electrons,” *Phys. Rev. X* **13**, 031001 (2023).
- [39] Shunya Konno, Warit Asavanant, Fumiya Hanamura, Hironari Nagayoshi, Kosuke Fukui, Atsushi Sakaguchi, Ryuhoh Ide, Fumihiro China, Masahiro Yabuno, Shigehito Miki, Hiroataka Terai, Kan Takase, Mamoru Endo, Petr Marek, Radim Filip, Peter van Loock, and Akira Furusawa, “Logical states for fault-tolerant quantum computation with propagating light,” *Science* **383**, 289–293 (2024).
- [40] Yi-Ru Chen, Hsien-Yi Hsieh, Jingyu Ning, Hsun-Chung Wu, Hua Li Chen, Zi-Hao Shi, Popo Yang, Ole Steuering, Chien-Ming Wu, and Ray-Kuang Lee, “Generation of heralded optical cat states by photon addition,” *Phys. Rev. A* **110**, 023703 (2024).
- [41] Rainer Blatt and David Wineland, “Entangled states of trapped atomic ions,” *Nature* **453**, 1008–1015 (2008).
- [42] D. Stoler, B.E.A. Saleh, and M.C. Teich and, “Binomial states of the quantized radiation field,” *Opt. Acta* **32**, 345–355 (1985).
- [43] Marios H. Michael, Matti Silveri, R. T. Brierley, Victor V. Albert, Juha Salmilehto, Liang Jiang, and S. M. Girvin, “New class of quantum error-correcting codes for a bosonic mode,” *Phys. Rev. X* **6**, 031006 (2016).
- [44] Ye-Hong Chen, Wei Qin, Roberto Stassi, Xin Wang, and Franco Nori, “Fast binomial-code holonomic quantum computation with ultrastrong light-matter coupling,” *Phys. Rev. Res.* **3**, 033275 (2021).
- [45] E. Alex Wollack, Agnetta Y. Cleland, Rachel G. Grunenke, Zhaoyou Wang, Patricio Arrangoiz-Arriola, and Amir H. Safavi-Naeini, “Quantum state preparation and tomography of entangled mechanical resonators,” *Nature* **604**, 463–467 (2022).
- [46] Yi-Hao Kang, Jie Song, and Yan Xia, “Error-resistant nonadiabatic binomial-code geometric quantum computation using reverse engineering,” *Opt. Lett.* **47**, 4099–4102 (2022).
- [47] Zhongchu Ni, Sai Li, Xiaowei Deng, Yanyan Cai, Libo Zhang, Weiting Wang, Zhen-Biao Yang, Haifeng Yu, Fei Yan, Song Liu, Chang-Ling Zou, Luyan Sun, Shi-Biao Zheng, Yuan Xu, and Dapeng Yu, “Beating the break-even point with a discrete-variable-encoded logical qubit,” *Nature* **616**, 56–60 (2023).
- [48] Juliette Soule, Andrew C. Doherty, and Arne L. Grimsmo, “Concatenating binomial codes with the planar code,” (2024), arXiv:2312.14390 [quant-ph].
- [49] Pei-Zhe Li, William J Munro, Kae Nemoto, and Nicolò Lo Piparo, “Continuous-variable multiplexed quantum repeater networks,” *Quantum Sci. Technol.* **10**, 025057 (2025).
- [50] En-Jui Chang, “High-rate extended binomial codes for multiqubit encoding,” *Phys. Rev. A* **112**, 032419 (2025).
- [51] Adithi Udupa, Timo Hillmann, Rabsan Galib Ahmed, Andrea Smirne, and Giulia Ferrini, “Performance of rotation-symmetric bosonic codes in the presence of random telegraph noise,” (2025), arXiv:2505.08670 [quant-ph].
- [52] Yuki Tanaka, Yuichiro Mori, Yuta Shingu, Aiko Yamaguchi, Tsuyoshi Yamamoto, and Yuichiro Matsuzaki, “Single-qubit rotations on a binomial code without ancillary qubits,” (2024), arXiv:2408.12968 [quant-ph].
- [53] S. Siddardha Chelluri, Sanchar Sharma, Frank Schmidt,

- Silvia Viola Kusminskiy, and Peter van Loock, “Bosonic quantum error correction with microwave cavities for quantum repeaters,” (2025), arXiv:2503.21569 [quant-ph].
- [54] Jordan Huang, Thomas J. DiNapoli, Gavin Rockwood, Ming Yuan, Prathyankara Narasimhan, Eesh Gupta, Mustafa Bal, Francesco Crisa, Sabrina Garattoni, Yao Lu, Liang Jiang, and Srivatsan Chakram, “Fast sideband control of a weakly coupled multimode bosonic memory,” (2025), arXiv:2503.10623 [quant-ph].
- [55] C.V. Sukumar and B. Buck, “Multi-phonon generalisation of the Jaynes-Cummings model,” *Phys. Lett. A* **83**, 211–213 (1981).
- [56] Surendra Singh, “Field statistics in some generalized Jaynes-Cummings models,” *Phys. Rev. A* **25**, 3206–3216 (1982).
- [57] A.S. Shumovsky, Fam Le Kien, and E.I. Aliskenderov, “Squeezing in the multiphoton Jaynes-Cummings model,” *Phys. Lett. A* **124**, 351–354 (1987).
- [58] Fam Le Kien, M. Kozierowski, and Tran Quang, “Fourth-order squeezing in the multiphoton Jaynes-Cummings model,” *Phys. Rev. A* **38**, 263–266 (1988).
- [59] W. Vogel and D.-G. Welsch, “ $k$ -photon Jaynes-Cummings model with coherent atomic preparation: Squeezing and coherence,” *Phys. Rev. A* **40**, 7113–7120 (1989).
- [60] Celso J. Villas-Boas and Daniel Z. Rossatto, “Multiphoton Jaynes-Cummings model: Arbitrary rotations in Fock space and quantum filters,” *Phys. Rev. Lett.* **122**, 123604 (2019).
- [61] Ricardo Puebla, Giorgio Zicari, Iñigo Arrazola, Enrique Solano, Mauro Paternostro, and Jorge Casanova, “Spin-boson model as a simulator of non-Markovian multiphoton Jaynes-Cummings models,” *Symmetry* **11**, 695 (2019).
- [62] Th. K. Mavrogordatos, “Cavity-field distribution in multiphoton Jaynes-Cummings resonances,” *Phys. Rev. A* **104**, 063717 (2021).
- [63] Pradip Laha, P. A. Ameen Yasir, and Peter van Loock, “Genuine non-gaussian entanglement of light and quantum coherence for an atom from noisy multiphoton spin-boson interactions,” *Phys. Rev. Res.* **6**, 033302 (2024).
- [64] Pradip Laha, P. A. Ameen Yasir, and Peter van Loock, “Tripartite multiphoton Jaynes-Cummings model: Analytical solution and Wigner nonclassicalities,” *Phys. Rev. A* **111**, 013710 (2025).
- [65] Frederick W. Strauch, Kurt Jacobs, and Raymond W. Simmonds, “Arbitrary control of entanglement between two superconducting resonators,” *Phys. Rev. Lett.* **105**, 050501 (2010).
- [66] S. Felicetti, D. Z. Rossatto, E. Rico, E. Solano, and P. Forn-Díaz, “Two-photon quantum Rabi model with superconducting circuits,” *Phys. Rev. A* **97**, 013851 (2018).
- [67] D. Leibfried, R. Blatt, C. Monroe, and D. Wineland, “Quantum dynamics of single trapped ions,” *Rev. Mod. Phys.* **75**, 281–324 (2003).
- [68] H. Häffner, C.F. Roos, and R. Blatt, “Quantum computing with trapped ions,” *Phys. Rep.* **469**, 155–203 (2008).
- [69] Pei-Zhe Li and Peter van Loock, “Memoryless quantum repeaters based on cavity-QED and coherent states,” *Adv. Quantum Technol.* **6**, 2200151 (2023).
- [70] Jacob Hastrup and Ulrik L. Andersen, “Protocol for generating optical Gottesman-Kitaev-Preskill states with cavity QED,” *Phys. Rev. Lett.* **128**, 170503 (2022).
- [71] D. M. Meekhof, C. Monroe, B. E. King, W. M. Itano, and D. J. Wineland, “Generation of nonclassical motional states of a trapped atom,” *Phys. Rev. Lett.* **76**, 1796–1799 (1996).
- [72] Max Hofheinz, E. M. Weig, M. Ansmann, Radoslaw C. Bialczak, Erik Lucero, M. Neeley, A. D. O’Connell, H. Wang, John M. Martinis, and A. N. Cleland, “Generation of Fock states in a superconducting quantum circuit,” *Nature* **454**, 310–314 (2008).
- [73] Yiwen Chu, Prashanta Kharel, Taekwan Yoon, Luigi Frunzio, Peter T. Rakich, and Robert J. Schoelkopf, “Creation and control of multi-phonon Fock states in a bulk acoustic-wave resonator,” *Nature* **563**, 666–670 (2018).
- [74] Fabian Wolf, Chunyan Shi, Jan C. Heip, Manuel Gessner, Luca Pezzè, Augusto Smerzi, Marius Schulte, Klemens Hammerer, and Piet O. Schmidt, “Motional Fock states for quantum-enhanced amplitude and phase measurements with trapped ions,” *Nat. Commun.* **10**, 2929 (2019).
- [75] Uwe von Lüpkke, Yu Yang, Marius Bild, Laurent Michaud, Matteo Fadel, and Yiwen Chu, “Parity measurement in the strong dispersive regime of circuit quantum acoustodynamics,” *Nat. Phys.* **18**, 794–799 (2022).
- [76] Sai Li, Zhongchu Ni, Libo Zhang, Yanyan Cai, Jiasheng Mai, Shengcheng Wen, Pan Zheng, Xiaowei Deng, Song Liu, Yuan Xu, and Dapeng Yu, “Autonomous stabilization of Fock states in an oscillator against multiphoton losses,” *Phys. Rev. Lett.* **132**, 203602 (2024).
- [77] Xiaowei Deng, Sai Li, Zi-Jie Chen, Zhongchu Ni, Yanyan Cai, Jiasheng Mai, Libo Zhang, Pan Zheng, Haifeng Yu, Chang-Ling Zou, Song Liu, Fei Yan, Yuan Xu, and Dapeng Yu, “Quantum-enhanced metrology with large Fock states,” *Nature Physics* **20**, 1874–1880 (2024).
- [78] Q. Rumman Rahman, Igor Kladarić, Max-Emanuel Kern, Luká š Lachman, Yiwen Chu, Radim Filip, and Matteo Fadel, “Genuine quantum non-gaussianity and metrological sensitivity of Fock states prepared in a mechanical resonator,” *Phys. Rev. Lett.* **134**, 180801 (2025).
- [79] Pradip Laha, Darren W. Moore, and Radim Filip, “Quantum coherence from a few incoherent bosons,” *Adv. Quantum Technol.* **6**, 2300168 (2023).
- [80] Suguru Endo, Yasunari Suzuki, Kento Tsubouchi, Rui Asaoka, Kaoru Yamamoto, Yuichiro Matsuzaki, and Yuuki Tokunaga, “Quantum error mitigation for rotation-symmetric bosonic codes with symmetry expansion,” *Phys. Rev. A* **111**, 062402 (2025).
- [81] E.T. Jaynes and F.W. Cummings, “Comparison of quantum and semiclassical radiation theories with application to the beam maser,” *Proc. IEEE* **51**, 89–109 (1963).
- [82] Bruce W. Shore and Peter L. Knight, “The Jaynes-Cummings model,” *J. Mod. Opt.* **40**, 1195–1238 (1993).
- [83] Jonas Larson and Themistoklis Mavrogordatos, *The Jaynes-Cummings Model and Its Descendants*, 2053–2563 (IOP Publishing, 2021).
- [84] Reinier W. Heeres, Brian Vlastakis, Eric Holland, Stefan Krastanov, Victor V. Albert, Luigi Frunzio, Liang Jiang, and Robert J. Schoelkopf, “Cavity state manipulation using photon-number selective phase gates,” *Phys. Rev. Lett.* **115**, 137002 (2015).
- [85] Pei-Zhe Li, Josephine Dias, William J. Munro, Peter van Loock, Kae Nemoto, and Nicolás Lo Piparo, “Performance of rotation-symmetric bosonic codes in a quantum repeater network,” *Adv. Quantum Technol.* **7**, 2300252

- (2024).
- [86] Yu-xi Liu, L. F. Wei, and Franco Nori, “Preparation of macroscopic quantum superposition states of a cavity field via coupling to a superconducting charge qubit,” *Phys. Rev. A* **71**, 063820 (2005).
- [87] David S. Schlegel, Fabrizio Minganti, and Vincenzo Savona, “Quantum error correction using squeezed Schrödinger cat states,” *Phys. Rev. A* **106**, 022431 (2022).
- [88] Pradip Laha, Lukáš Slodička, Darren W. Moore, and Radim Filip, “Thermally induced entanglement of atomic oscillators,” *Opt. Express* **30**, 8814–8828 (2022).
- [89] Pradip Laha, “Dynamics of a multipartite hybrid quantum system with beamsplitter, dipole-dipole, and Ising interactions,” *J. Opt. Soc. Am. B* **40**, 1911–1921 (2023).
- [90] Pradip Laha, Darren W. Moore, and Radim Filip, “Entanglement growth via splitting of a few thermal quanta,” *Phys. Rev. Lett.* **132**, 210201 (2024).